Fluvial features on Titan: Insights from morphology and modeling

Devon M. Burr[1,†], J. Taylor Perron[2], Michael P. Lamb[3], Rossman P. Irwin III[4], Geoffrey C. Collins[5], Alan D. Howard[6], Leonard S. Sklar[7], Jeffrey M. Moore[8], Máté Ádámkovics[9], Victor R. Baker[10], Sarah A. Drummond[1], and Benjamin A. Black[2]

[1]*Earth and Planetary Sciences Department, University of Tennessee–Knoxville, 1412 Circle Drive, Knoxville, Tennessee 37996-1410, USA*

[2]*Department of Earth, Atmospheric, and Planetary Sciences, Massachusetts Institute of Technology, 77 Massachusetts Avenue, Cambridge, Massachusetts 02139, USA*

[3]*Geological and Planetary Sciences, California Institute of Technology, 1200 E California Boulevard, MC 170-25, Pasadena, California 91125, USA*

[4]*Center for Earth and Planetary Studies, National Air and Space Museum, Smithsonian Institution, MRC 315, 6th Street at Independence Avenue SW, Washington, District of Columbia 20013, USA*

[5]*Physics and Astronomy Department, Wheaton College, 26 E. Main Street, Norton, Massachusetts 02766, USA*

[6]*Department of Environmental Sciences, University of Virginia, P.O. Box 400123, Charlottesville, Virginia 22904-4123, USA*

[7]*Department of Geosciences, San Francisco State University, 1600 Holloway Avenue, San Francisco, California 94132, USA*

[8]*Space Sciences Division, National Aeronautics and Space Administration Ames Research Center, MS 245-3, Moffett Field, California 94035, USA*

[9]*Astronomy Department, University of California, 601 Campbell Hall, Berkeley, California 94720-3411, USA*

[10]*Department of Hydrology and Water Resources, The University of Arizona, J.W. Harshbarger Building, Room 246, 1133 E. James E. Rogers Way, Tucson, Arizona 85721-0011, USA*

ABSTRACT

Fluvial features on Titan have been identified in synthetic aperture radar (SAR) data taken during spacecraft flybys by the *Cassini* Titan Radar Mapper (RADAR) and in Descent Imager/Spectral Radiometer (DISR) images taken during descent of the *Huygens* probe to the surface. Interpretations using terrestrial analogs and process mechanics extend our perspective on fluvial geomorphology to another world and offer insight into their formative processes. At the landscape scale, the varied morphologies of Titan's fluvial networks imply a variety of mechanical controls, including structural influence, on channelized flows. At the reach scale, the various morphologies of individual fluvial features, implying a broad range of fluvial processes, suggest that (paleo-)flows did not occupy the entire observed width of the features. DISR images provide a spatially limited view of uplands dissected by valley networks, also likely formed by overland flows, which are not visible in lower-resolution SAR data. This high-resolution snapshot suggests that some fluvial features observed in SAR data may be river valleys rather than channels, and that uplands elsewhere on Titan may also have fine-scale fluvial dissection that is not resolved in SAR data. Radar-bright terrain with crenulated bright and dark bands is hypothesized here to be a signature of fine-scale fluvial dissection. Fluvial deposition is inferred to occur in braided channels, in (paleo)lake basins, and on SAR-dark plains, and DISR images at the surface indicate the presence of fluvial sediment. Flow sufficient to move sediment is inferred from observations and modeling of atmospheric processes, which support the inference from surface morphology of precipitation-fed fluvial processes. With material properties appropriate for Titan, terrestrial hydraulic equations are applicable to flow on Titan for fully turbulent flow and rough boundaries. For low-Reynolds-number flow over smooth boundaries, however, knowledge of fluid kinematic viscosity is necessary. Sediment movement and bed form development should occur at lower bed shear stress on Titan than on Earth. Scaling bedrock erosion, however, is hampered by uncertainties regarding Titan material properties. Overall, observations of Titan point to a world pervasively influenced by fluvial processes, for which appropriate terrestrial analogs and formulations may provide insight.

INTRODUCTION

Observations of Titan from the *Cassini-Huygens* mission to the Saturn system (Kerridge et al., 1992; Matson et al., 2002) revealed an extraterrestrial world with an active volatile cycle and resultant fluvial landforms. Analysis of fluvial landforms on Earth by the founders of modern geology (e.g., Lyell, 1830) laid the groundwork for a better understanding of terrestrial landscape evolution. The discovery of relict valley networks and outflow channels on Mars (Mars Channel Working Group, 1983) fundamentally revised our view of that planet's evolution and early history. Likewise, the revelation of fluvial features on Titan provides a powerful tool to better understand the geologic history of this largest satellite of Saturn.

On both Mars and Titan, fluvial features have been inferred through their planform similarity to terrestrial fluvial networks, a type of analogical reasoning common in planetary geology (Mutch, 1979) and all sciences (Hess, 1966). One pitfall with analogical reasoning is equifinality, in which different causative processes yield similar effects (Mutch, 1979; Schumm, 1991). An illustration from planetary science is the past debate over the volcanic or impact origin of lunar craters. This directionality, whereby landscapes are first encountered remotely at low

[†]E-mail: dburr1@utk.edu

GSA Bulletin; March/April 2013; v. 125; no. 3/4; p. 299–321; doi: 10.1130/B30612.1; 7 figures; 1 table.

resolution and only later (if at all) at outcrop scale, is the inverse of the traditional directionality for terrestrial geology. It makes planetary geology particularly susceptible to the effects of equifinality because the low resolution limits discernment of key characteristics. As corroborative input to geologic analogs, mathematical models are strong analogs in which attributes and physical laws are expressed in a simplified formulation that can be compared to the landscape under study. Models also provide versatility in attribute parameters, which is critical for extraterrestrial investigations.

The largest contribution of the Mars Channel Working Group (1983) to understanding Mars developed a decade after the first *Mariner 9* images were returned from that planet, where fluvial features were formed by flowing water eroding and transporting silicate rock and sediment, as on Earth. Almost a decade has now passed since the *Cassini-Huygens* mission first returned images from Titan, where fluvial features are formed by flowing liquid alkanes (primarily methane) acting on materials derived from an icy crust and organic-rich atmosphere. As with Mars, understanding of fluvial features on Titan is advanced through analogy to terrestrial features and application of mechanical principles. The distinct materials and very different conditions on Titan highlight the need for morphologic analogies to be supported by physical theory.

This paper presents an analysis of fluvial processes on Titan through both qualitative interpretation of spacecraft images and quantitative theory. In the first part of the paper, we review and analyze the morphology of fluvial features observed in *Cassini-Huygens* data. In the second part, we present an overview and discussion of Titan's "alkanology" (dynamics and cycling of hydrocarbons), including precipitation and runoff production. In the third part, we articulate the theoretical underpinnings of both hydraulic and sedimentologic processes likely to occur on Titan. The concluding summary includes suggestions of high-priority areas for future investigations.

TITAN'S FLUVIAL LANDFORMS

Questions of Formation Mechanism and Extent

Fluvial features have been mapped in data from the three *Cassini* surface-imaging instruments, namely, the Imaging Science Subsystem (ISS; best map resolution ~1–2 km/pixel; Porco et al., 2004, 2005), the Visual and Infrared Mapping Spectrometer (VIMS; best map resolution ~1 km/pixel; Brown et al., 2004; Barnes et al., 2007a), and the *Cassini* Titan Radar Mapper (RADAR; Elachi et al., 2004, 2005) (Fig. 1). Of these three data sets, fluvial features have been most extensively observed in synthetic aperture radar (SAR) data (examples in Fig. 2) from the RADAR instrument. These images have the best combination of map resolution (best map resolution ~300 m/pixel) and coverage (~40% of the surface to date) for observing fluvial networks, and they were collected at a wavelength similar to the size of fluvial cobbles observed on the surface (Tomasko et al., 2005). Although fluvial features were inferred from early VIMS data (Barnes et al., 2007b; Jaumann et al., 2008), more recent work has not shown a strong global correlation between fluvial features mapped from SAR and from VIMS data (Langhans et al., 2012). Fluvial networks have also been mapped in higher-resolution visible light images (~20–90 m/pixel) taken by the Descent Imager/Spectral Radiometer (DISR; Tomasko et al., 2005) (Fig. 3) on the *Huygens* probe during its descent to the Titan surface. Jaumann et al. (2009) provide a detailed overview of the characteristics of the *Cassini-Huygens* surface-sensing data sets for Titan.

Because of the difference in data set resolutions, the mapped fluvial features give contrasting impressions regarding formation as river channels versus river valleys. The individual features observed in the SAR data are of order 0.5–1 km in width, with maximum reported widths of ~3 km to ~10 km (Lorenz et al., 2008a). Based on their curvilinear appearance, networked morphology, and radar shadowing, which implies negative relief, these features have been generally referred to as channels (Porco et al., 2005; Elachi et al., 2006; Barnes et al., 2007b; Lorenz et al., 2008a). In contrast, the individual features in DISR images, with roughly an order of magnitude better resolution, show widths of ~30 m (Tomasko et al., 2005; Perron et al., 2006). Terrestrial rivers may carve and be inset within much wider valleys or canyons, such as the Colorado River within the Grand Canyon, and similar fluvial morphologies have been observed in high-resolution images of Mars (e.g., Irwin et al., 2005). By analogy, these *Huygens* DISR features have been inferred to be river valleys that contain channels (Perron et al., 2006).

Distinguishing channels from valleys is vital for correct estimates of fluvial processes and effects, including the correct estimation of liquid and sediment discharge. At SAR resolution, diagnostic channel features such as stream banks and bed forms are not resolved, and shading by valley walls and differences in reflectivity of surface materials contribute to difficulty in direct interpretation of fluvial features. In many cases, the appearances of Titan fluvial features in SAR data are equally consistent with interpretations as river valleys as they are with the more commonly published interpretation as channels. We discuss interpretations of individual fluvial landforms in the section Individual Fluvial Landforms Observed in SAR Data.

The fine-scale fluvial networks observed in the DISR image mosaic (Fig. 3) are not discernible in SAR data (Soderblom et al., 2007b; Jaumann et al., 2009), raising a second question as to the extent of fine-scale fluvial dissection on Titan. Based on mapping using SAR data, ~1% of Titan's surface was inferred to be covered by fluvial landforms (Lorenz et al., 2008a; Lopes et al., 2010) with endogenic and other exogenic processes shaping the remaining surface. However, an alternative interpretation of Titan's global landscape is formation entirely by exogenic processes (Moore and Pappalardo, 2011). Some regions on Titan show a distinctive texture in SAR images of alternating brighter and darker kinked, wrinkled, or crenulated banding (e.g., Figs. 2A, 2B, 2F, and 2G). Although fluvial networks are typically not discernible in this crenulated terrain, they are often adjacent to or connected with it, suggesting a possible genetic relationship. We discuss our hypothesis that the crenulated terrain on Titan is fluvial dissected in the section Crenulated Terrain: Evidence of Fine-Scale Fluvial Dissection.

These discussions are presented by decreasing scale, beginning with networks observed in SAR data, followed by individual features observed in SAR data, then the networks observed in DISR data, and finally the crenulated terrain.

Fluvial Networks Observed in SAR Data

Fluvial network morphology or drainage pattern provides geologic information at the landscape scale, including substrate lithology and permeability, structural features, and landscape topography (e.g., Howard, 1967; Twidale, 2004). Classes of drainage patterns have pervasive characteristics that distinguish them from other basic patterns, although modified or transitional patterns may have spatially varying characteristics of multiple patterns. Howard (1967) and Ichoku and Chorowicz (1994) presented examples of both basic and modified patterns.

Network drainage pattern analysis has proven to be valuable in planetary studies for multiple reasons. It is applicable to networks composed of either river channels or river valleys, which is helpful for low-resolution data, where the exact nature of the fluvial features cannot be discerned (cf. Pieri, 1979). Drainage pattern analysis is valid at a range of map resolutions, so even in the likely event that low-order (distal or "finger-

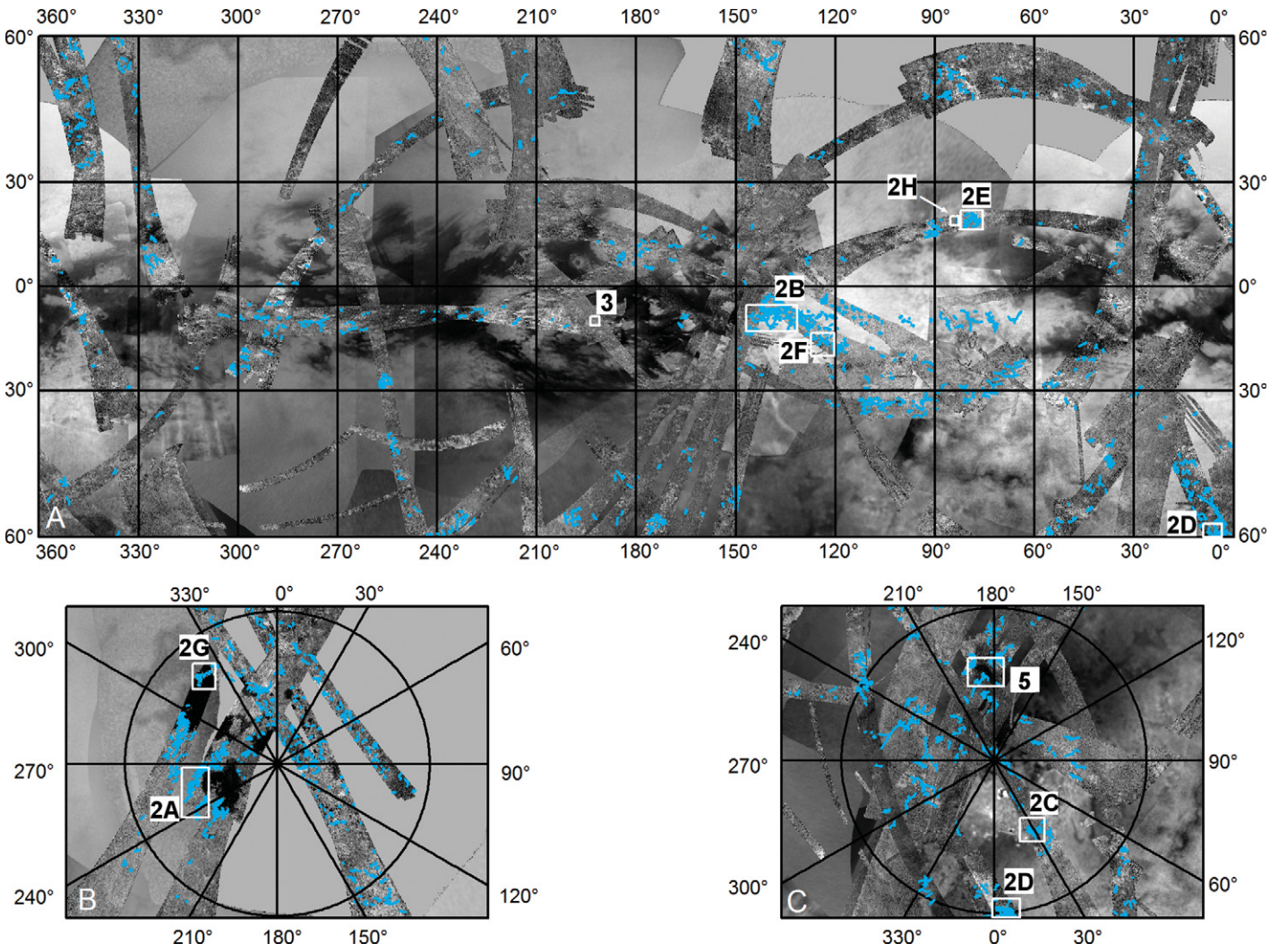

Figure 1. Global mosaic using *Cassini* Imaging Science Subsystem (ISS) data (lower layer) and *Cassini* Titan Radar Mapper (RADAR) synthetic aperture radar (SAR) data up through T71 (upper layer), with fluvial features mapped on SAR data shown in blue. White boxes show locations of subsequent figures as identified by adjacent lettering. (A) Fluvial features from 60°N to 60°S. (B) Fluvial features in the north polar region, 60°N to 90°N. (C) Fluvial features in the south polar region, 60°S to 90°S. Scale varies across image, 10° longitude or 10° at the equator is equal to ~450 km.

tip") tributaries are not discernible, the approach still provides accurate information (e.g., Ichoku and Chorowicz, 1994). Such analysis provides information over the region covered by the discernible network, whereas information from channel patterns (e.g., straight, meandering, braided, anastomosing, anabranching) is commonly more restricted in area.

The range of terminology applied to drainage patterns on Titan hints at a range of hydrologic controls on channelized runoff (Baugh, 2008; Lorenz et al., 2008a; Langhans et al., 2012). Given the surprisingly Earth-like nature of Titan's surface (e.g., Coustenis and Taylor, 2008) and calculations suggesting similar fluvial erosion and transport processes on Earth and Titan (Collins, 2005; Burr et al., 2006), the existing terrestrial drainage pattern terminology may be usefully applied to Titan fluvial networks, in order to more precisely identify and suggest implications for each network class. Application to Titan networks of a quantitative terrestrial classification algorithm (Ichoku and Chorowicz, 1994) yields rectangular, dendritic, and parallel network morphologies (Burr et al., 2009b). Rectangular networks constitute the majority of Titan's networks (Drummond et al., 2012), including networks adjacent to Kraken and Ligeia Maria (Cartwright et al., 2011) (e.g., Figs. 2A and 2B). While each network morphology carries important geologic implications (e.g., Howard, 1967; Twidale, 2004; for a summary, see Drummond, 2012), the rectangularity characterizing the majority of networks suggests control by tectonic structures and associated topography. Analysis of the shape of some well-resolved north polar networks indicates that these networks have produced only minor erosional modification of the surface, suggesting either recent resurfacing or slow fluvial incision (Black et al., 2012).

Individual Fluvial Landforms Observed in SAR Data

Individual fluvial features in SAR data from Titan may be grouped into six morphological classes using the basic qualitative parameters of radar backscatter (bright or dark), relative width (narrow or wide), and relative length (stubby or long). This classification scheme,

based on readily observable plan-view attributes, yields a limited number of classes for which specific hypotheses may be proposed. The following discussion describes those six classes and offers some interpretations (summarized in Table 1). Type examples of the six classes are shown in Figure 2, with their locations indicated on Figure 1.

We include Shreve magnitudes (i.e., the number of headwater links upstream of a given link) in these class descriptions, rather than in the previous network discussion, because we find that the magnitudes vary by the class of the individual links comprising the network. In comparison to the Horton-Strahler stream-ordering technique, Shreve magnitudes provide a measure of topology that gives a better indication of discharge from runoff (Knighton, 1998). Because of SAR image speckle and resolution limits, the apparent Shreve magnitudes reported here almost certainly underestimate the true values. Nonetheless, these values are provided as a measure of relative network integration. The magnitudes reported here are several times higher than stream orders reported previously for Titan networks observed in SAR data (Lorenz et al., 2008a; Langhans et al., 2012), due to the inherent differences in use of stream order versus link magnitude and possibly to the "segmented storage of valleys in the database" of previous work.

1. Narrow, long, radar-dark features can be found either as individual sinuous landforms or as well-developed networks, such as those observed in the north polar vicinity of Ligeia Mare (Fig. 2A). Apparent Shreve magnitudes of the prominent networks in this area range from ~20 to ~70, and the most extensive of these networks is ~340 km in length. Junction angles are moderate to high (up to 90°). Although width varies considerably with location in the network, the main (trunk) links are ~0.5 km wide. A general lack of radar shadowing, observable as light-dark pairing, suggests fairly shallow depths and/or shallowly sloping walls, although shadowing may be obscured by the radar-dark tone. Many of these features terminate at dark areal features interpreted as hydrocarbon lakes (Stofan et al., 2007), as seen near 74°N, 246°W (Fig. 2A; other locations indicated in Fig. 1).

Interpretations: The morphology of networks of narrow radar-dark features indicates tributary flow, with moderate to high tributary junction angles suggesting low-terrain slopes and/or structural influence (Drummond et al., 2012). The dark tone may result from deposition of fine-grained material (Lorenz et al., 2008a). A drape of fine grains implies either consistently low-energy flow, possibly due to low slopes, or a hydrograph with a low-flow tail, which may result from an extended or irregularly shaped drainage basin area (Knighton, 1998). Alternatively, the dark tone may indicate a smooth bed of sand-sized particles, the availability of which is inferred from the presence of extensive tropical dunes (e.g., Radebaugh et al., 2007b). Available coverage indicates that radar-dark fluvial features may be concentrated at higher latitudes, although the degree and significance of this concentration have not yet been quantified. If substantiated, this concentration may indicate a greater supply of fine-grained organic sediment poleward, contrary to what might be expected from the concentration of organic-rich dunes in the tropics (Radebaugh et al., 2007b;

Figure 2 (*on following page*). Examples of the six morphological classes for individual fluvial features. On all figures, solid small black arrows indicate *Cassini* Titan Radar Mapper (RADAR) illumination directions. (A) Examples of narrow, long, radar-dark features near 74°N, 246°W. The dark tone of these features is interpreted here as a deposit of fine-grained material. The dark area to the north (right) is Ligeia Mare. Filled white arrows point to inferred drowned valleys (Stofan et al., 2007), with the width of the submerged region narrowing headward. The hollow white arrow points to a partially drowned river valley system. Area of crenulated terrain is visible immediately south (left) of the mare. The rectangular drainage pattern suggests formation on landscapes affected by tectonic structures (Drummond et al., 2012). (B) Examples of narrow, long, radar-bright features near 10°S, 137°W, in western Xanadu. The bright tone in the fluvial features is interpreted as resulting from internal reflections from debris with diameters larger than the RADAR wavelength (2.17 cm) (LeGall et al., 2010). This region illustrates the interspersion of darker units within lighter, inferred rougher terrain, suggesting embayment of the rougher terrain by fine-grained deposits. The visible fluvial network is an example of a rectangular drainage pattern (Burr et al., 2009b; Drummond et al., 2012). Crenulated terrain, hypothesized to be finely fluvially dissected, is visible at the upper-left portion of the image. (C) An example of a wide, long, radar-dark feature near 74°S, 27°W. The dark tone may be due in some locations to inherently radar-dark material (e.g., the floor of the main trunk) and elsewhere to radar shadowing (e.g., the western side of main trunk valley), although the distinction between these two causes is not clear everywhere. Based on the radar shadowing, this feature is hypothesized here to be an incised bedrock channel or confined meandering river set within a river valley formed by erosion. (D) A second example of a wide, long, radar-dark feature near 59°S, 5°W, proposed to be a distributary channel (Lorenz et al., 2008a) and hypothesized here to be a braided or an anabranching network. (E) Examples of wide, long, radar-bright features near 20°N, 80°W, named Elivagar Flumina. Narrower ends originate on a dark surface, inferred to be smooth plains material, and wider ends terminate at smooth, radar-bright terrain, inferred to be sedimentary deposits with debris on the scale of or larger than the RADAR wavelength (2.17 cm). In accordance with previous work (Lorenz et al., 2008a), we hypothesize these features to be gravel-bed, braided, ephemeral rivers that terminate in alluvial deposits. (F) Examples of wide, long, radar-bright features near 18°S, 122°W, northeastern Tui Regio. These features are proposed to have roughness elements on the same scale as or larger than the 2.17 cm wavelength of the RADAR (Le Gall et al., 2010). The wider ends originate from crenulated terrain (upper right), inferred to be rough upland, and the narrow ends disappear on a dark surface (lower left), inferred to be smooth plains. The origination of this fluvial feature at maximum width from the crenulated terrain indicates that the crenulated terrain has contributing fluvial features below the image resolution. A few of these tributaries are visible as connected zigzag traces at upper left and center right. (G) Examples of stubby, radar-dark features (in white ovals) near 69°N, 298°W, around the southern margin of Kraken Mare (dark area at upper right). Shorelines having "sinuous extensions" are described as being similar in appearance to drowned river valleys on Earth (Stofan et al., 2007). Portions of the radar-bright terrain with the brightest return have crenulated texture. (H) Examples of stubby, radar-bright features (white oval) on the eastern rim and wall of Menrva crater near 20°N, 83°W. The black box marks the location of the inset image at upper right, showing an individual feature with bright and dark regions (white and black arrows), which are located distal from and proximal to the radar illumination direction (from upper left), indicating radar illumination and shadowing, respectively. Between the dark and bright regions, there is a region of intermediate brightness (gray arrow), inferred to be a rough floor.

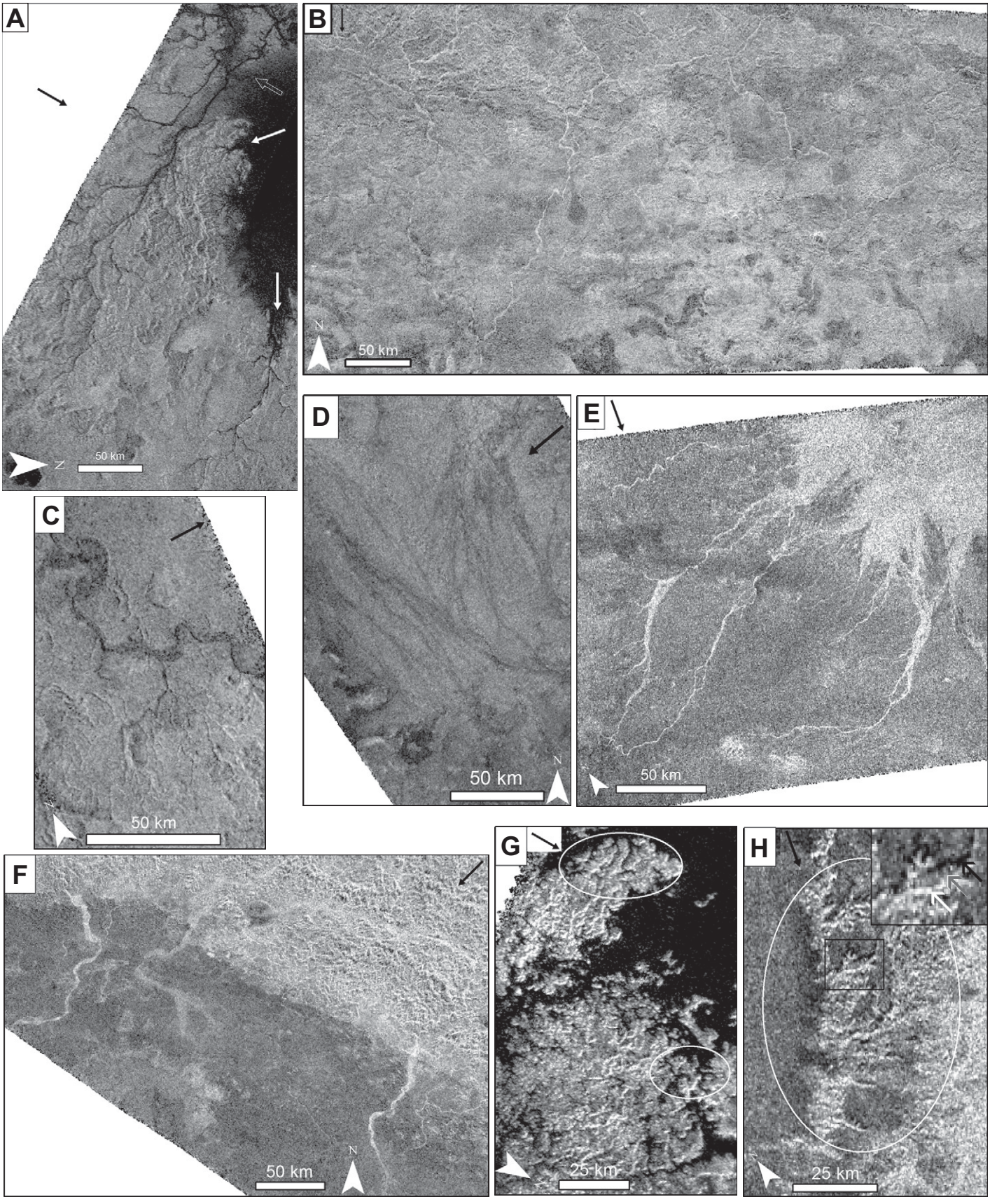

Figure 2.

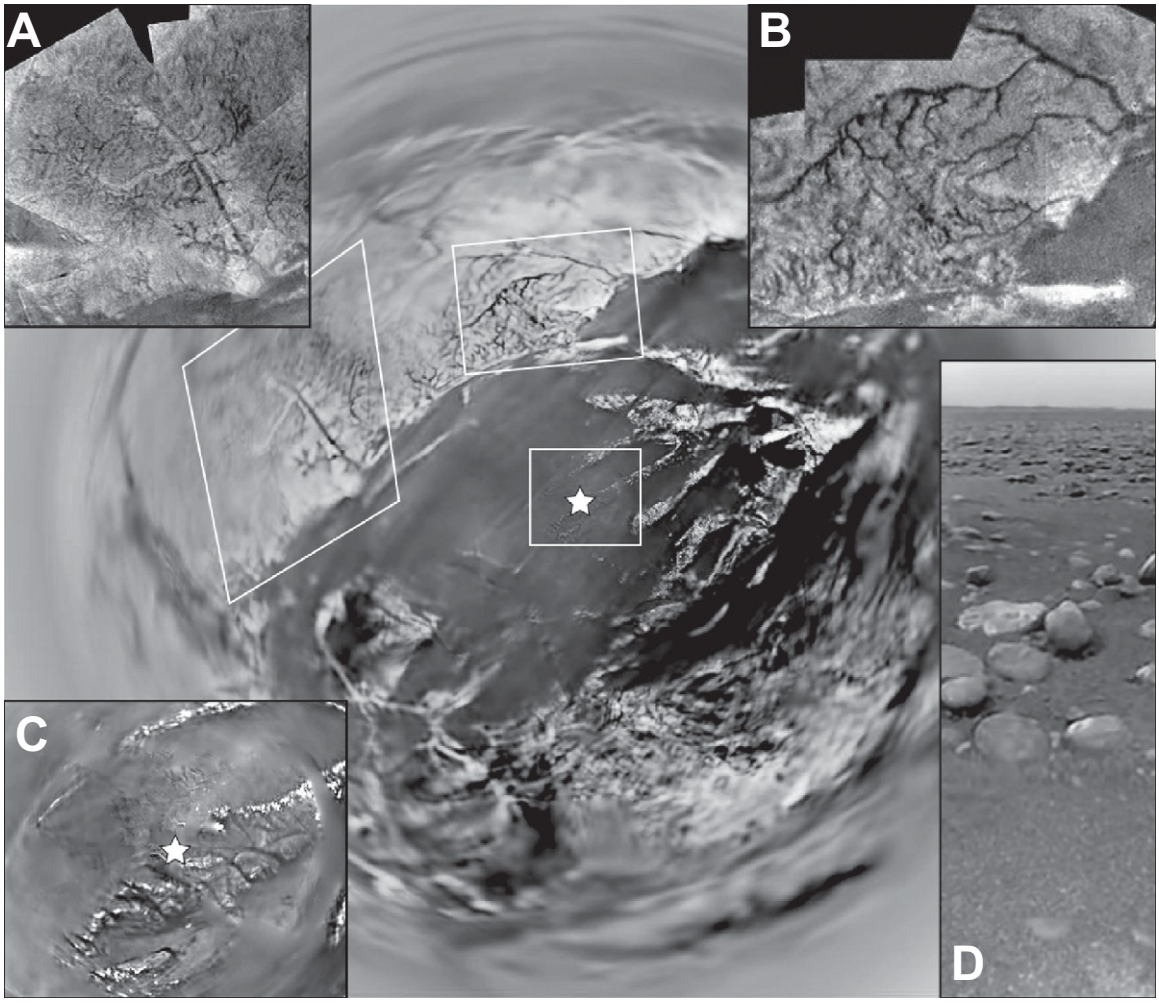

Figure 3. *Huygens* Descent Imager/Spectral Radiometer (DISR) mosaics of features around the *Huygens* probe landing site, at ~10°S, 168°E. Background: stereographic projection of the view from 6 km above the surface, centered on the landing site, marked with a star. North is up. Scale varies across image. White boxes show the approximate extents of insets A–C. Insets: (A) Western drainage networks. Image width is ~8 km. (B) Northern drainage networks. Image width is ~6 km. (C) Stereographic projection of the landing site from 600 m above the surface. Image width is ~2 km. (D) View from the landing site, looking toward the horizon. Diameter of the largest clasts in middle distance is ~15 cm. Dark zones stretching to the right from clasts in the middle distance suggest scour tails. All images are courtesy of National Aeronautics and Space Administration (NASA)/Jet Propulsion Laboratory (JPL)/European Space Agency (ESA)/U. Arizona.

Barnes et al., 2008), and it would indicate complex global sediment supply and/or transport.

2. Narrow, long, radar-bright features have dimensions similar to the radar-dark features discussed in point 1. They often form well-developed networks with apparent Shreve magnitudes up to ~40. Bright networks in western Xanadu observed in the overlapping T13 (Lorenz et al., 2008a) and T44 swaths (Fig. 2B) range from ~250 km to 400 km in total length, and the individual features are ~0.75 km and ~1.5 km wide.

Interpretations: The bright appearance indicates significant radar backscatter, for which the most likely explanation at present is considered to be icy rounded rocks larger in size than the radar wavelength (2.17 cm) acting as natural radar retro-reflectors (Le Gall et al., 2010). Grains (pebbles and cobbles) of this size were observed at the *Huygens* landing site (Tomasko et al., 2005), demonstrating the production and transport of such material. Thus, radar-bright fluvial features are hypothesized to be river valleys with debris a few centimeters or larger in size (Lorenz et al., 2008a). Relative radar brightness on the sides of fluvial features that face the illumination direction (e.g., smallest tributaries in Fig. 2C) may result from radar illumination of the valley walls.

3. Wide, long, radar-dark features are similar in tone and length to their narrow counterparts, but they are several times wider (~2.5–5 km). They may be subdivided by morphology and geographic location into two groups. In polar regions, they occur as branching networks with enlarged main trunks, which often show radar shadowing and illumination patterns (e.g., Fig. 2C). As seen in this example, smaller tributaries may likewise show evidence of shadowing and be radar-dark, though not universally so. These networks of wide radar-dark features, like those composed of narrow radar-dark links, commonly terminate in inferred lakes or other

TABLE 1. SUMMARY OF THE SIX PROPOSED MORPHOLOGICAL CATEGORIES, POSSIBLE INTERPRETATIONS, AND EXAMPLE FIGURES*

Morphological class	Hypothesized interpretations	Example figures
Narrow, long, radar-dark	• River valleys, the dark tone of which is due to deposition of finer-grained particles from low-energy flow, resulting from low slopes and/or extended or irregularly shaped drainage basin; possibly some shadowing of steep-sided valley walls	Figure 2A
Narrow, long, radar-bright	• River valleys, the bright tone of which is due to internal reflections by debris larger than the RADAR wavelength (2.17 cm); possibly some illumination of steep-sided valley walls	Figure 2B
Wide, long, radar-dark	1. Sinuous features with radar shadowing hypothesized to be incised bedrock channels *or* confined meandering stream valleys (e.g., Fig. 2C) 2. Straighter features lacking radar shadowing and conjoined in braided networks hypothesized as anabranching channels with possible terminal splays where features widen (e.g., Fig. 2D)	Figures 2C and 2D
Wide, long, radar-bright	1. Features originating on dark plains and terminating in radar-bright, homogeneous terrain hypothesized to be gravel-bed, braided, ephemeral rivers terminating at fluvial deposits (e.g., Fig. 2E) 2. Features originating in radar-bright, crenulated terrain and terminating in dark plains hypothesized to be braided rivers draining mountainous, dissected landscapes (e.g., Fig. 2F)	Figures 2E and 2F
Stubby, radar-dark	• River valleys formed by a headward retreat mechanism • Dark tone due to fill by dark tholins and/or drowning by liquid, possibly shadowing of steep-sided slopes	Figure 2G
Stubby, radar-bright	• River valleys formed by a headward retreat mechanism • Bright tone due to illumination of valley walls; intermediate-toned pixels due to rough material on valley floor	Figure 2H

*See "Titan's Fluvial Landforms" section for further details.

depositional basins. At lower latitudes, observed wide, radar-dark features may lack radar shadowing, have less-well-defined edges, tend to be straighter, and form networks with an intertwined appearance, having multiple conjoined features and faint lineations within the features (e.g., Fig. 2D). For these networks, boundaries are poorly defined, and apparent Shreve magnitudes are low.

Interpretations: The wide, radar-dark features shown in Figure 2D were speculated to be channels with fine-grained deposits (Lorenz et al., 2008a). Lack of apparent radar shadowing, indicative of shallowly sloping sides, along with individual link and networked morphologies, suggests a braided or possibly anabranching network of low width-to-depth, multithread channels. The multiple subparallel features, if they connote a distributary network, would suggest depositional processes within and adjacent to these channels. For example, sites where the dark features widen might be indicative of terminal splays, deposits that form in dryland fluvial-lacustrine systems where a river debouches into a playa lake or onto its floodplain (Graf, 1988).

For the other group of wide, radar-dark features, which are commonly found near the poles (e.g., Fig. 2C), shadowing and illumination indicative of steep side slopes and a sinuous planform pattern support an interpretation as incised bedrock channels or confined meandering rivers set within river valleys formed by erosion. Incised channels may have point bar or other deposits of finer-grained alluvial fill, suggested by radar-dark material distributed at various locations (bends) within the feature. Meandering channels require some cohesion of the bank material, which on Earth is associated with plants (Davies and Gibling, 2010a, 2010b). As on Mars (Burr et al., 2009b, 2010), putative meandering channels on Titan would require a nonbiological cohesion mechanism. This cohesion mechanism may be common; data from the *Huygens* Surface Science Package (SSP) show that the material at the *Huygens* landing site may have been cohesive at the time of landing (Lorenz et al., 2009; Atkinson et al., 2010).

4. Wide, long, radar-bright features have dimensions similar to their darker counterparts (~200–300 km in length, ~4.5–6 km in width), and they can have a similar intertwined or multithread appearance with diffuse boundaries. These features appear to form only poorly developed networks (apparent Shreve magnitudes <10) or individual landforms. Widths often vary noticeably along the features. The narrower ends terminate in radar-dark terrain, inferred to be smooth plains material, and the wider ends commonly abut radar-bright terrain. This radar-bright terrain, where homogeneous in tone, has been interpreted as either cryovolcanic or alluvial (e.g., Fig. 2E; see Lopes et al., 2007). In other cases, the radar-bright terrain may have a crenulated appearance (Fig. 2F), which has been interpreted as mountainous (Lopes et al., 2010; Radebaugh et al., 2011).

Interpretations: The lack of radar shadowing, suggesting only shallow incision into the plains, along with their intertwined planform appearance and variable width (Lorenz et al., 2008a; Lopes et al., 2010), suggests anabranching, anastomosing, or braided channels. Thus, wide, long, radar-bright networks may include the most likely river channels seen in SAR data. In such multithread channels, the flowing liquid would be unlikely to simultaneously occupy the full width of the feature as resolved in SAR data.

We hypothesize the radar-bright features that terminate at homogeneous bright terrain (Fig. 2E) to be gravel-bed, braided, ephemeral rivers (e.g., Bridge and Lunt, 2006) and their terminal gravelly deposits. Terrestrial braided streams have weak banks, an abundant supply of bed load, highly variable discharge, and high stream power (Knighton, 1998), which together can create irregular widening and narrowing, as observed in Figure 2E. This interpretation implies commonly sub-bankfull flow in these multithread channels with a low discharge per unit channel width. Terrestrial braided channels are typically straighter in overall planform than streams formed in cohesive alluvium, which may meander or anabranch, so low sinuosity in these instances does not necessarily imply either structural control or strong banks.

We hypothesize that the radar-bright features that terminate at crenulated bright terrain (e.g., Fig. 2F) are likewise braided channels, based on similar morphological observation, but with the inverse flow direction relative to the adjacent bright terrain. The bright, crenulated terrain, interpreted as mountainous (Lopes et al., 2010), is inferred to be the source region for these braided channels. In these cases of bright features draining crenulated terrain, the decrease in width and tone with distance may be due to a decrease in discharge due to evaporation and/or infiltration over the dark plains material. Alternatively, the change in appearance may result from comminution of sediment to sizes smaller than the radar wavelength.

Thus, the wide, long, radar-bright features, like their radar-dark counterparts, may be subdivided into two groups (Table 1). For these features, however, the basis for the division is the appearance—homogeneous or crenulated—

of the adjacent radar-bright terrain. These two subgroups of radar-bright features are less distinctive in appearance than the radar-dark subgroups, and both are found at low latitudes.

5. Stubby, radar-dark features range from ~1.5 km to 3 km in length. These features are found individually or as poorly developed networks (apparent Shreve magnitudes of 2–5). Stubby, radar-dark features are found, for example, near 69°N, 298°W around the perimeter of Kraken Mare (Fig. 2G).

Interpretations: The stubby shape of these features suggests formation by some mechanism of headward retreat of the inferred channel. Such retreat occurs by waterfall erosion where a strong capping layer overlies a weak substrate or where rocks have pervasive vertical joints, or by groundwater seepage erosion in loose or weakly cemented sediment (Lamb et al., 2006, 2008a; Lamb and Dietrich, 2009). The dark tone may indicate fill by dark tholins or organic hydrocarbons (Soderblom et al., 2007a; Barnes et al., 2008) or possibly shadowing in steep-sided valleys (for discussion of how to test for shadowing effects, see Soderblom et al., 2007b). In cases where the radar-dark features debouch into basins or plains, the continuity between radar-dark basin material and the dark stubby features suggests tholin deposition by backwater in or drowning of the contributing valleys (Stofan et al., 2007).

6. Stubby, radar-bright features tend to be larger than stubby, radar-dark features (~20 km in length) and have poorly developed branching (apparent Shreve magnitudes also of 2–5), as seen on the eastern rim of Menrva crater near 20°N, 83°W (Fig. 2H). Although mostly radar-bright, these features also show subparallel radar-dark regions, with some intermediate-toned pixels in between. These bands of different radar tone trend roughly orthogonal to illumination direction (Fig. 2H).

Interpretations: The stubby appearance again suggests formation by some mechanism of headward retreat. The orientation and bands of bright and dark tone are inferred to be areas of radar illumination and radar shadowing, respectively. The interspersed pixels of intermediate tone suggest a region of rough material on the feature floor, such as debris loosened from the surrounding wall rock by weathering and/or incision during overland flow.

Our interpretations of the different classes of fluvial features visible in SAR data (see also Table 1) have implications for the likely relationships between observed feature width and the actual (paleo-)flow width. We interpret the narrow, long features as river valleys, for which valley widths likely exceed flow widths. The different SAR albedos (bright or dark) are attributed to different types of sedimentary fill (rounded icy cobbles or finer-grained particles, respectively). The wide, long, dark features with shadowing may be confined meandering streams or incised bedrock channels, for which flow widths again would be less than observed widths. The straighter, shallower features in this class are interpreted as braided or anabranching multichannel systems. The wide, long, bright features are hypothesized to be either ephemeral braided rivers terminating at bright deposits, or braided multichannel rivers fed from dissected mountainous terrain and terminating on dark plains. For none of these various multichannel systems would the flow be likely to occupy all the channels. Stubby features are inferred to be valleys produced by headward erosion, for which flow would occupy only a fraction of the width.

Fluvial Landforms Observed in DISR Data

At considerably smaller scale, valley networks observed in DISR images have two distinct morphologies. The networks to the north of the *Huygens* landing site (Fig. 3B) are more sinuous, originate close to topographic divides, and show downstream increases in valley width. In contrast, the networks to the west of the *Huygens* landing site (Fig. 3A) have straighter main-stem valleys, larger tributary junction angles, shorter tributaries, and possibly more enlarged dark areas around the valley heads (Tomasko et al., 2005; Perron et al., 2006). This morphological contrast has been interpreted as evidence for disparate formation processes, with the more northern networks interpreted as having a distributed atmospheric source for the flow (Perron et al., 2006), and the western networks having formed through groundwater sapping due to subsurface flow of methane (Tomasko et al., 2005; Soderblom et al., 2007b).

Inferences about groundwater sapping based solely on valley network morphology are problematic. On Earth, field studies of putative groundwater sapping networks incised into competent bedrock have revealed no clear evidence that spring discharge can form valleys without overland flow, and they indicate that surface runoff has contributed substantially to network formation (Lamb et al., 2007, 2008a). If thick deposits of unconsolidated, permeable material mantle Titan's surface, (e.g., Soderblom et al., 2009; Waite et al., 2009), then groundwater sapping might play a role in forming valley networks, as it can on Earth in such settings (Dunne and Black, 1980; Howard, 1988; Schumm et al., 1995; Perron and Hamon, 2012). However, if sapping formed the western networks in the DISR mosaic, then it would imply that the substrate in that area has substantially different mechanical properties than the substrate underlying the northern networks. No independent evidence to suggest such a contrast in subsurface materials is observed.

With a water-ice crust that is far below its melting temperature and minimally soluble in hydrocarbons (Lorenz and Lunine, 1996), Titan's fluvial valleys are unlikely to be the product of thermal erosion or dissolution (Perron et al., 2006). If the surface is composed partly of organic compounds with very different physical properties, then melting or karst may have played a part in shaping the surface topography, as has been suggested for the polar lakes (Stofan et al., 2007; Bourgeois et al., 2008), but no such compounds have yet been identified. In view of the erosive capability of overland flow and the abundant independent evidence of atmospheric precipitation, we consider erosion by precipitation-fed runoff to be the more likely formation mechanism for both the northern and western networks.

The straighter valleys and more orthogonal tributary junction angles of the western network have also been interpreted as the result of structural or tectonic control of valley incision (Tomasko et al., 2005; Soderblom et al., 2007b; Jaumann et al., 2009). This interpretation is plausible, especially in view of the identification from SAR data of rectangular fluvial networks elsewhere on Titan (Burr et al., 2009b; Drummond et al., 2012). Such morphologic correlations are not unique, however. Straight valleys on Earth may form where flow directions are enforced by preexisting topography (which may be tectonic in origin), and orthogonal tributary junctions are frequently observed where a trunk stream incises rapidly or channel longitudinal profiles are strongly concave-up (Horton, 1945; Schumm, 1956; Howard, 1971).

The valley networks near the *Huygens* landing site terminate at a boundary between the bright, elevated, fluvially dissected area, and the dark, low-lying area in which the probe landed (Fig. 3). The boundary resembles a shoreline, but the dark area contained no pooled liquid at the time of landing (Zarnecki et al., 2005; Keller et al., 2008). In north polar lakes, the inferred drowned fluvial networks (e.g., Fig. 2G) (Stofan et al., 2007) appear to record changes in lake levels, and paleolake clusters have been hypothesized for low-latitude sites (Moore and Howard, 2010). This evidence of substantial changes in the volume of liquid surface reservoirs elsewhere on Titan supports the hypothesis that the boundary at the *Huygens* landing site was once a shoreline or some transitional zone between an erosional surface and a depositional one.

It is not known whether the observed fluvial features near the *Huygens* landing site are typical of Titan's surface. However, the greater abundance of lakes (Hayes et al., 2008), fluvial networks (Drummond et al., 2012; Langhans et al., 2012), and cloud activity (Porco et al., 2005) at the poles suggests that the probe landing site in the tropics could have sparse fluvial dissection relative to polar regions. Jaumann et al. (2009) summarized observations of the landing site in coarser-resolution *Cassini* images, showing how difficult it is to discern the fluvial features in the SAR data, even when those features are known to exist. This comparison underscores the value of *Huygens* observations, showing that the apparent scarcity of fine-scale fluvial features in *Cassini* images should not be construed as evidence of their absence. Hence, we turn to a discussion of landscapes in SAR images that might be signatures of fine-scale, fluvially dissected landscapes, even if drainage networks are not resolved.

Crenulated Terrain: Evidence of Fine-Scale Fluvial Dissection

In *Cassini* SAR images, much of the bright highlands (e.g., Xanadu) has repeated bright and dark crenulated bands with apparent widths of ~2–6 km (e.g., Figs. 2A, 2B, 2F, and 2G). Through visual similarity to a SAR image of the Himalayas, this crenulated banding was suggested to be a possible expression of fluvial dissection (Radebaugh et al., 2007a). In some locations, obvious fluvial networks are embedded in the crenulated terrain. These fluvial features may debouch onto dark plains (Fig. 2F) or into lakes (Fig. 2A), but they become indiscernible with distance headward (i.e., into the crenulated terrain). However, multiple lines of reasoning support the inference that crenulated terrain is a heavily dissected landscape of channels and adjacent valley slopes.

Comparison of SAR and DISR Images

As noted already, SAR data do not resolve the *Huygens* landing site networks that are visible in the DISR images (Fig. 3) (Jaumann et al., 2009), highlighting the possibility of unresolved fine-scale fluvial dissection elsewhere on Titan.

Tributary Nature of Networks

The dendritic, parallel, and rectangular drainage patterns identified on Titan (Burr et al., 2009b; Drummond et al., 2012) are tributary, implying that the observable links must have lower-order tributaries feeding into them.

Visibility of Some Tributaries

A few lower-order tributaries are visible within the crenulated terrain, feeding into broad fluvial features that stretch onto dark plains (cf. Lopes et al., 2010), as shown in Figure 2F. These few examples substantiate the possibility that many additional tributaries exist within the crenulated terrain.

Terrestrial Analogs

A comparison of SAR images and topography for two variously dissected terrestrial landscapes illustrates the difficulty of identifying fine-scale drainage networks even in high-resolution SAR data (e.g., Farr et al., 2007). Topography of a finely dissected region of the Allegheny Plateau, shown in a shaded relief image (Fig. 4A), exhibits obvious hierarchical drainage networks. The main valleys of these networks are also easily visible in a SAR image, but even in this highly dissected landscape with high-relief valleys, the low-order tributaries are somewhat obscured (Fig. 4B). In a landscape that may be more comparable to some locations on Titan, a region of Michigan's Upper Peninsula, which was heavily modified by the Laurentide ice sheet, shows partial dissection by low-relief fluvial networks that empty into Lake Superior. This geographic relationship between the fluvial networks and terminal lake basins is similar to that of the fluvial features that terminate at Titan's north polar lakes (e.g., Fig. 2A). The terrestrial fluvial topography is again identifiable in a shaded relief image (Fig. 4C). However, only a few of these features are visible as faint lineations or crenula-

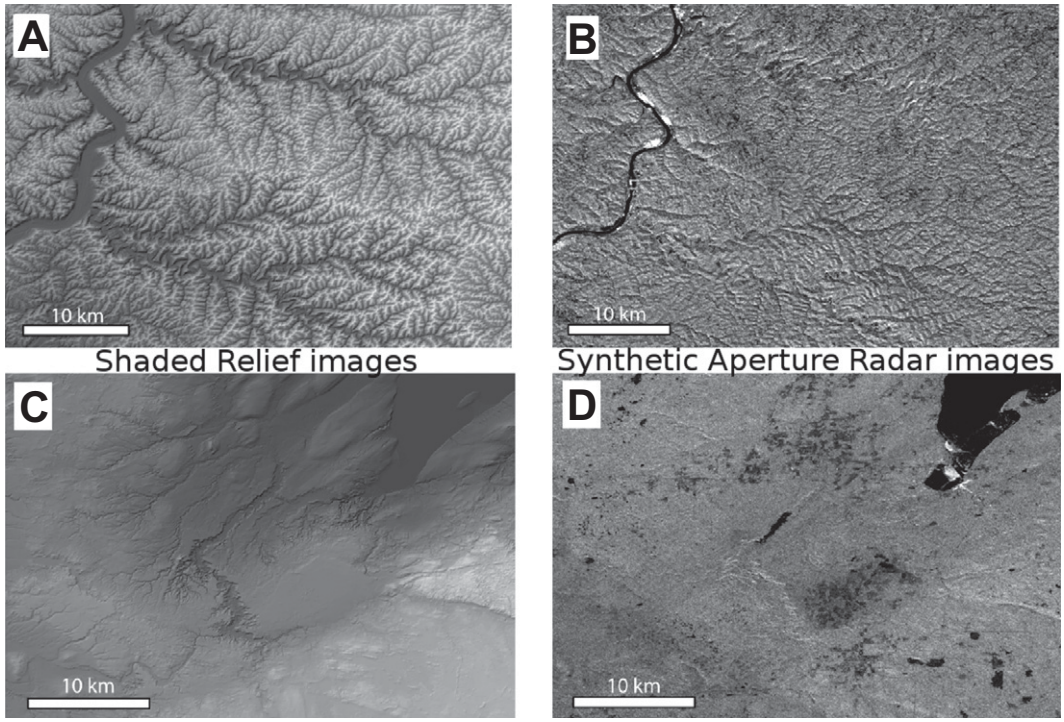

Figure 4. Comparison of synthetic aperture radar (SAR) images and topography for terrestrial drainage networks. (A) Topography shown as a shaded relief image and (B) SAR image of the region southwest of L'Anse Bay, Lake Superior, on Michigan's Upper Peninsula, centered at 46.57°N, 88.67°W. (C) Topography shown as a shaded relief image and (D) SAR image of a section of the Allegheny Plateau east of the Ohio River in northern West Virginia and southwest Pennsylvania, centered at 39.67°N, 80.70°W. SAR images are from the C-band antenna on board the Shuttle RADAR Topography Mission (Farr et al., 2007). Topography is from the U.S. Geological Survey National Elevation Data Set. Map projections are transverse Mercator, with a pixel size of ~30 m. Figure is modified from Black et al. (2012).

tions in a SAR image with comparable spatial resolution (Fig. 4D). Thus, in both of these examples, fluvial networks that are readily apparent in topographic data are underrepresented in SAR images. That terrestrial SAR images with much higher resolution than *Cassini* SAR data can obscure fluvial features suggests that fluvial dissection on Titan may be much more extensive than is apparent in SAR images.

Not all SAR images of crenulated terrain show obvious valley networks, and not all bright highlands exhibit obvious crenulations. However, the inability of SAR images to resolve the intricate drainage network imaged by DISR suggests that many or most of these bright highlands, whether obviously crenulated or not, are fluvially dissected at a scale too fine to be resolved in SAR data. The radar-bright "hummocky and mountainous terrain" unit is inferred to cover ~12% of Titan's surface as mapped up to T30 (Lopes et al., 2010). If this percentage can be accurately extrapolated to the entire body, then greater than a tenth of the surface of Titan—an order of magnitude higher than the previous estimates (Lorenz et al., 2008a; Lopes et al., 2010)—may be dissected by fluvial features.

Depositional Environments

Evidence of fluvial sediment transport and deposition on Titan appears at a variety of scales as observed in both *Huygens* and SAR data. Potential sources of sediment, including tools for incision, are discussed under "Bedrock Erosion" later herein.

Local Sedimentary Deposits

Huygens data offer hints about the processes operating on the Titan landscape. Stereo-topography indicates that the valley walls north of the landing site approach the angle of repose for cohesionless material (Tomasko et al., 2005; Soderblom et al., 2007b), suggesting that the landscape is being actively dissected, and that mass wasting may be an important hillslope sediment production and transport mechanism. DISR images of the landing site show a ground surface completely mantled with sediment (Fig. 3D; Tomasko et al., 2005). The *Huygens* SSP penetrometer measurements indicate a soft, solid surface with a stronger upper layer and a weaker subsurface, consistent with either a crust or a layer of coarse sediment over finer-grained sediment (Zarnecki et al., 2005; Keller et al., 2008; Atkinson et al., 2010). The observed surface grain-size distribution includes particle sizes ranging from roughly 3 mm, the smallest diameter resolvable by the camera, up to 15 cm (Tomasko et al., 2005), i.e., grain sizes that could be moved by fluvial flow (Burr et al., 2006; see also Figs. 6 and 7A). Images collected just before landing resolved meter-size boulders near the landing site, although none was visible from the surface (Tomasko et al., 2005). Grains at the surface have been rounded, perhaps by mechanical abrasion during energetic fluvial transport consistent with possible scour tails (Fig. 2D) or by in situ chemical weathering of the water-ice and soluble organic compounds as indicated by spectra of the site (Tomasko et al., 2005; Jacquemart et al., 2008; Schröder and Keller, 2008).

Regional Sedimentary Landforms

SAR images reveal probable fluvial sedimentary depositional environments that appear to be analogous to terrestrial braid plains, alluvial fans, and depositional basins. Several valley systems terminate in fan-like forms with fluvial features that broaden, split, and appear to braid (e.g., Figs. 2D–2F). In some cases, topographic data demonstrate that these fan-like forms occur in regional lows, supporting their identification as alluvial fans (e.g., Moore and Howard, 2010). In general, neither the mechanism(s) of emplacement of sedimentary deposits—whether from rivers or debris flows (cf. Blair and McPherson, 1994)—nor the grain-size characteristics of the deposits are known, although high radar backscatter for some fluvial features (i.e., those shown in Fig. 2F) suggests the presence of grains larger than the radar wavelength of 2.17 cm (Le Gall et al., 2010). Many of the depositional landforms are radar-bright, suggesting an abundance of particles greater in size than the RADAR wavelength.

In some regions, radar-bright fluvial networks in crenulated uplands are interspersed with darker, smooth-textured areas that may connect to adjacent fluvial links (e.g., Fig. 2B). In other regions, similar radar-dark terrain, with fluvial features terminating within it, appears to embay the brighter terrain (e.g., Fig. 2F). Some of this radar-dark terrain, parts of which belong to the plains units of Lopes et al. (2010), is likely to be deposits from the fluvial features that are adjacent to or terminate within it.

Lacustrine Deposits

Multiple *Cassini* instruments have identified alkane lakes and inferred paleolakes (e.g., Stofan et al., 2007; Brown et al., 2008; Turtle et al., 2009) into which fluvial features terminate. The lake boundaries exhibit a variety of morphologies, from highly irregular shorelines adjacent to crenulated terrain ("terrestrial flooded river valleys"; Stofan et al., 2007) to smoother shorelines for lakes within plains units. Where valley systems enter lakes with smooth shorelines, they sometimes terminate at or adjacent to broad platforms (e.g., Fig. 5). Because the alkane lakes are only partially transparent to radar illumination (e.g., Hayes et al., 2008, 2010, 2011), these inferred fluvial features gradually fade with distance lakeward. On the basis of plan-view morphology and variation (fading) in tone, these features are hypothesized to be fluvial fans or deltaic deposits (e.g., Moore and Howard, 2010; Wall et al., 2010).

TITAN ALKANOLOGY

To the extent that the terrestrial analogs for the fluvial features on Titan are valid, they require atmospheric and near-surface processes to create the channelized surface flow. Here,

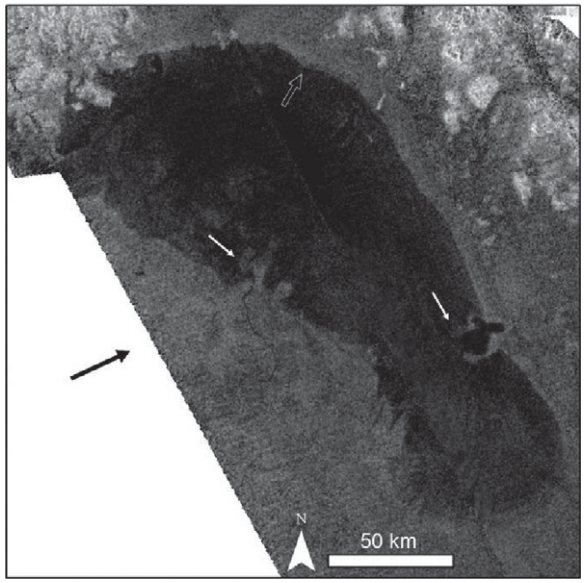

Figure 5. Ontario Lacus in the south polar region of Titan, centered near ~72°S, 183°W. Outlined arrow within the lake shows a smooth shoreline. White arrows point to inferred fluvial deposits at the mouth of valleys debouching into the lake. Sub-lake topography is suggested in some portions of the lake, including shallowly submerged topography in the western and southern areas. Solid black arrow indicates *Cassini* Titan Radar Mapper (RADAR) illumination direction.

we consider relevant atmospheric processes and possible near-surface pathways by which liquid may be supplied to the surface. We group these processes and pathways under the term "alkanology," defined here as the occurrence, circulation, distribution, and properties of alkanes on Titan and in its atmosphere, including precipitation and runoff production.

Precipitation Characteristics

Volatile Sources

Although the photochemical dissociation of methane in Titan's atmosphere leads to irreversible methane loss over ~10–100 m.y. (Flasar et al., 1981; Yung et al., 1984), the lack of strong carbon isotopic fractionation in methane (Niemann et al., 2005) indicates that the atmospheric methane is continually resupplied. As on Earth, the resupply of atmospheric volatiles is complex. Some evidence is consistent with a subsurface source of methane: The surface was measured to be "damp" by the *Huygens* probe (Lorenz and Lunine, 2006), and some surface features suggest geologically recent cryovolcanic activity (Sotin et al., 2005; Nelson et al., 2009a, 2009b; Wall et al., 2009; Lopes et al., 2010). Other evidence suggests surface sources: Models of atmospheric circulation and weather patterns require a surface source (e.g., Mitchell, 2008), and evaporation from polar lakes (see Mitri et al., 2007; Lopes et al., 2010) is implied by the detection of south polar fog (Brown et al., 2009) and changes in lake shorelines (Turtle et al., 2009; Hayes et al., 2011).

Droplet Size

From these sources, Titan's atmosphere is estimated to hold several meters of precipitable methane (e.g., Tokano et al., 2006), relative to only a few centimeters of precipitable water at Earth (Gao et al., 2004), so optically thick clouds at Titan are expected. *Voyager* infrared (IR) spectra suggest cloud drop sizes in excess of 50 μm, therefore classifiable as rain (Toon et al., 1988). Later telescopic spectroscopy (Griffith, 2000) and direct imaging (Brown et al., 2002; Roe et al., 2002) both show clouds. Early raindrop models predicted evaporation of the droplets in the atmosphere, i.e., virga (Lorenz, 1993), but suggestions of "raindrop splashes" (Karkoschka et al., 2007), although later discounted (Karkoschka and Tomasko, 2009), provide motivation for revisiting this conclusion. Modeling of ternary mixtures of methane-ethane-nitrogen (Graves et al., 2008) and modeling of cloud microphysics (Barth and Rafkin, 2007; Barth and Rafkin, 2010) both predict that rainfall droplets grow large enough to reach the surface. Laboratory experiments show that supercooled ethane droplets may be stabilized by the absorption of methane gas, such that 1 μm droplets would have lifetimes of hours to days before freezing (Wang et al., 2010).

Rainfall Rate

Rainfall rates on Titan have been estimated through various approaches. Simple models equating an assumed energy available for convection to either latent heat or to work done in dissipating the drag on falling raindrops yield maximum mean annual rainfall of 0.6 cm to ~2 cm (Lorenz, 2000; Lorenz and Rennó, 2002). More advanced models tend to give lower estimates: a one-dimensional (1-D) cloud microphysics model predicts a precipitation rate of ~0.2 cm/yr (Barth and Toon, 2006), and a two-dimensional (2-D) global circulation model with a deep reservoir of surface methane gives a mean annual precipitation rate of ~0.5 cm/yr (Mitchell, 2008). Conversely, the general circulation model (GCM) of Tokano et al. (2001) predicts globally averaged rates of up to 10 cm/yr, although rainfall at particular times and places would be affected by temporal and elevation effects (Barth, 2010), precipitation-evaporation balances, putative cryovolcanic outgassing of methane, and other factors. Recent three-dimensional (3-D) simulations show that significant precipitation of several millimeters per day can occur near the equator at equinox (Mitchell et al., 2011; Schneider et al., 2012), consistent with observations (Turtle et al., 2011).

Rainfall rate information can also be derived for particular locations from the observed effects on the surface. DISR data provide constraints on flow width, sediment grain size, drainage area, and slope for the fluvial networks northwest of the *Huygens* landing site (Fig. 3B). Using these data as constraints in a model of runoff, channel flow, and grain entrainment, Perron et al. (2006) calculated rainfall rates of 0.05–1.5 cm/h to move the observed sediment sizes. This range of values for this specific location fits within the two-order-of-magnitude range of global values given by numerical models.

Storm rainfall in mass per area can be converted into rainfall rates using the density of liquid methane (taken as 450 kg/m^3) and storm duration. Complex 3-D mesoscale microphysical models of Titan storms predict maximum methane rainfall of 110 kg/m^2 ("equivalent to flash floods"; Hueso and Sánchez-Lavega, 2006), which equates to ~6–8 cm/h for a 3–4 h storm. Application of a modified terrestrial cloud model with additional microphysics shows significant rain accumulation (20–30 kg/m^2) over a 5 h period, with peak accumulations in excess of 100 kg/m^2 (Barth and Rafkin, 2007), yielding an average rainfall rate of ~1 cm/h or a peak rate of ~5 cm/h.

Frequency of Fluvially Significant Events

The frequency of precipitation events that lead to surface modification can be constrained by modeling and observations. Simple thermodynamic modeling suggested rainstorms on Titan may occur only every millennium (Lorenz et al., 2005). However, observations of surface changes in ISS data over Titan's equatorial region are attributed to methane storm precipitation, inferred to occur seasonally (Turtle et al., 2011). From DISR data, the calculated rainfall rates of 0.05–1.5 cm/h, in conjunction with an assumed 2 h storm duration and modeled yearly rainfall rates (Tokano et al., 2001; Barth and Toon, 2006), yield estimated recurrence intervals for erosive runoff events ranging from once per Titan season (~6 Earth yr) to once per Earth day (Perron et al., 2006). Observations demonstrate spatially and temporally uneven rainfall on Titan, where it is likely seasonally controlled (e.g., Schneider et al., 2012), so similar data on sediment size, topography, and channel geometry would be required to make similar estimates elsewhere on Titan.

Precipitation Patterns

Modeled

In general, model precipitation occurs in areas of methane reservoirs and large-scale updrafts associated with surface-level convergence, where adiabatic cooling tends to result in condensation (Mitchell et al., 2006). Assuming an infinite surface reservoir, various models have reproduced observed cloud formation as resulting from upwelling following transport of moisture toward the summer pole (Tokano et al., 2001; Mitchell et al., 2006; Rannou et al., 2006). Idealized 2-D and 3-D GCMs with shallow (7 m) global surface reservoirs make predictions that are consistent with most observations, including some seasonal variability (Mitchell, 2008; Mitchell et al., 2011). Including (sub) surface methane transport in such models explains the north polar clustering of (paleo)lakes, low-latitude storm intensities at equinox, and the observed distribution of southern clouds (Schneider et al., 2012).

Observed

Earth-based near-infrared (IR) spectra showed enhanced opacity, attributed to condensed methane clouds near ~30 km altitude and methane drizzle at lower altitudes, localized near Xanadu (Ádámkovics et al., 2007, 2009). In the north polar region, nondetection of clouds in *Cassini* radar observations rules out storms at the time of the observation (during the winter) and limits persistent drizzle to less than ~10 cm/yr (Lorenz et al., 2008b).

Large cloud outbursts observed both in ISS and telescopic data have occurred at the southern summer pole near solstice (Porco et al., 2005; Schaller et al., 2006), with equatorial storms near equinox (Schaller et al., 2006; Turtle et al., 2011). The evolution of a large midlatitude storm was recorded by both ground-based and spacecraft observations (Ádámkovics et al., 2010). Surveys of cloud coverage during the *Cassini-Huygens* prime mission are broadly consistent with circulation models (Rodriguez et al., 2009, 2011; Brown et al., 2010).

Surface and Near-Surface Flow Paths

Lakes cover only a few percent of Titan's surface (e.g., Stofan et al., 2007), so most precipitation would fall on land. As on Earth, rainfall could evaporate from, infiltrate into, or flow across the surface to a fluvial network. Runoff in networks can arrive via channel precipitation, saturation overland flow, Hortonian overland flow, shallow subsurface flow, and base flow.

Stream channels comprise a few percent or less of a watershed's area, but precipitation into the channels and adjacent flooded areas can contribute up to ~30% of a flood event's peak discharge, because the supply is not delayed (Dingman, 1970; Beven and Wood, 1993; Crayosky et al., 1999). In a terrestrial study, the largest percentages of channel precipitation as a fraction of peak discharge occurred during dry-season flood events (Crayosky et al., 1999).

Rainfall onto saturated areas with emerging groundwater generates saturation overland flow, which can also enter the channel quickly due to the commonly low position of saturated areas in the watershed (Dunne and Black, 1970). Saturation overland flow is common in humid regions on Earth where water tables are maintained near the land surface. Concave hillslope profiles, wide valley floors, convergent topography on hillslopes, and perched saturated layers are important sources of saturation overland flow (Ward, 1984).

Hortonian overland flow occurs when the precipitation rate exceeds the surface infiltration capacity (Horton, 1933, 1945), and it develops during intense storms on fine-grained soils or impermeable surfaces. It contributes significantly to streamflow in dryland areas, where precipitation commonly occurs as storms, soil may be compacted, and low water tables do not favor saturation overland or groundwater contributions (Yair and Lavee, 1985).

Precipitation may also infiltrate and move as shallow subsurface flow. Typically, infiltrated water moves too slowly to contribute significantly to the intermittent flood discharges that dominate river channel morphometry. However, subsurface storm flow can be significant in high-permeability zones near streams.

Base flow, which also has a groundwater source, fluctuates over longer periods and has little dependence on individual precipitation events (e.g., Dingman, 2002).

Application to Titan

The infiltration capacity and depth to the fluid table are uncertain for Titan, so the relative importance of channel precipitation, overland flow, and subsurface flow is unknown. The event floods that dominate river channel morphometry are also a function of climate, recent precipitation history, and storm intensity, which may be highly variable on Titan. In observations to date (over approximately one-quarter of a Titan year), the largest cloud bursts have occurred at the southern (summer) pole (Porco et al., 2005; Schaller et al., 2006), consistent with models showing migration of the intertropical convergence zone (ITCZ) between the summer poles (Tokano, 2011). Particularly if antecedent conditions are dry, intense storms offer the greatest potential for precipitation to exceed infiltration and generate Hortonian overland flow. As the south (summer) polar convection migrates northward, short-term surface changes due to precipitation have been documented near Titan's equator (Turtle et al., 2011), where the rapid changes might have been produced by Hortonian overland flow over low-permeability sediments, e.g., tholins. The distribution of saturated areas near channels is unknown, but the occurrence of high-latitude lakes suggests the potential for saturated areas and saturation overland flow in the polar regions.

Runoff Production

Runoff production is equal to the stream discharge divided by the contributing area. Event runoff (above base flow, if any) represents precipitation minus infiltration, evaporation, and attenuation of flow over the contributing surface, all of which may vary during an individual storm. Assuming losses by these three mechanisms to be negligible, Perron et al. (2006) calculated a minimum precipitation rate of 0.05–1.5 cm/h in the watershed shown in their figure 2 (our Fig. 3B), in order to generate their estimated discharge. Lorenz et al. (2008a) used a 10-km-wavelength bend, assumed to be a meander, in inferring a discharge of ~5000 m^3/s from a contributing area of roughly 80 by 30 km, deriving ~1 cm/h of runoff. Jaumann et al. (2008) calculated that measured "channel" (possibly valley) widths and discharge estimates from scaled empirical relationships imply 0.06–6 cm/h of precipitation and therefore runoff from storms.

These results, though imprecise, are similar to theoretical precipitation rates in individual storms (see previous section, Precipitation Characteristics). However, the *Cassini* radar data often cover only part of a watershed, and the sparseness of topographic data complicates mapping of drainage divides, so measurements of contributing area are often uncertain and may be low. Surface attenuation can be negligible in small drainage basins (see examples in Perron et al., 2006), but it can also be significant, especially at larger scales. Thus, runoff estimates should be interpreted as maxima.

Rarity of precipitation appears to be the most direct cause of aridity at Titan's equator, perhaps due to interpolar migration of the ITCZ (Tokano, 2011), but high evaporation rates for methane (Mitri et al., 2007; Tokano, 2009) may also remove fluid from the (near-)surface, affecting the hydrologic response during the next event. Some terrestrial landscapes are arid because evaporation is high more than because precipitation is low. In northern Australia, the summer monsoon delivers 0.5–1.5 m/yr of rain, but annual potential evaporation is 2.0–2.6 m. The potential moisture deficit averaged across the continent is considerably higher, with annual rainfall of 0.47 m and potential evaporation of 3.25 m (Nanson et al., 2002).

On Titan, despite the much lower solar radiation, annual evaporation rates for methane are similar to evaporation of water from terrestrial lakes. Calculated methane evaporation rates of 0.3–10 m/yr are consistent with its relative humidity in Titan's atmosphere and the fractional surface area covered by lakes (Mitri et al., 2007) and with observed changes in lake levels (Hayes et al., 2008). The fraction of rainfall that is shed as runoff varies widely in terrestrial dryland watersheds, but evaporation from the surface or soil can be more significant than runoff as a water loss mechanism. In the Colorado River drainage basin, for example, only 3.3 cm of the total 36 cm annual average precipitation is lost as runoff (Graf, 1988). By analogy, evaporation from watershed surfaces on Titan may be a more significant fluid-loss mechanism than runoff.

Discharge

Once runoff becomes channelized, it is characterized by the discharge, estimated as the product of flow width, flow depth, and depth-averaged flow velocity, which is a function of channel slope, gravity, and the friction exerted by the channel on the liquid (see Eq. 2 in the next section). Order-of-magnitude estimates of discharge on Titan have been derived from measured dimensions of fluvial features or the likely size of transported sediment (Perron

et al., 2006; Jaumann et al., 2008; Lorenz et al., 2008a). However, the flow depth, channel slope, or friction factor values are poorly constrained for Titan (with the exception of the topography of the fluvial networks imaged by the DISR, discussed previously). In addition, the flow width is imprecise because the nature of the fluvial features—whether channels or valleys—is uncertain. For these reasons, the usual approach is not straightforward to apply.

An alternative approach uses empirical relationships between width or meander wavelength and dominant discharge from studies of terrestrial channels (see summary by Knighton, 1998). This approach is valid only for the range of variables from which the empirical function was derived (Williams, 1988) and requires measurement of channel (not valley) dimensions. The nature of the features might be constrained by comparison with wavelength/width ratios for alluvial channels, which typically fall within a narrow range for Earth (~10–14; Leopold and Wolman, 1960). However, this range of values may not pertain to sinuous bedrock valleys with inset channels (Dury, 1964, 1985), as the bedrock valley dimensions may reflect much larger, rarer floods (Baker, 1977; Kochel, 1988; Wohl, 2000). For resistant bedrock valleys, the bank erodibility is low and the recovery time may be very large, so the most geomorphically effective flood may have a long recurrence interval, even by Titan's standards (Lorenz et al., 2005).

MODELING HYDRAULICS, FLUVIAL EROSION, AND SEDIMENT TRANSPORT

On Earth, fluvial morphology results from feedbacks among fluid flow, sediment supply and transport, and topography. The existence of fluvial features on Titan and the terrestrial analogs discussed herein suggest that similar processes are at work there. Sediment flux in terrestrial rivers may be supply-limited or transport-limited (e.g., Howard et al., 1994). In a supply-limited river, the sediment flux is a function of erosion of bedrock in the riverbed, delivery of sediment from neighboring hillslopes or upstream reaches, and atmospheric deposition. Thus, the sediment flux q_s is limited by the amount of material supplied to the flow, i.e., $q_s < q_{sc}$, where q_{sc} is the volumetric sediment transport capacity of the river per unit channel width. Under these conditions, riverbeds contain partial or full exposure of bedrock, and river channels tend to be net erosional. Although some progress has been made to understand the mechanics of supply-limited rivers (for a review, see Whipple, 2004), knowledge is limited in comparison to transport-limited systems. In a transport-limited river, the sediment flux is determined by the capacity of the flow to transport the material (i.e., $q_s = q_{sc}$). Thus, sediment flux can be estimated from flow hydraulics alone. These riverbeds tend to be fully alluviated (i.e., no exposed bedrock) and can be net depositional, bypass, or erosional, depending on the time scale of interest.

We begin the discussion with the better-studied and constrained transport-limited systems carrying a predominantly undissolved (solid) load. In this regime, the sediment transport is highly dependent on the stresses within the flowing fluid, and we consider the dynamics of fluid flow first.

Flow Characteristics

The effects of flow of a Newtonian fluid in a channel can be modeled through conservation equations for fluid mass and momentum and a parameterization for bed friction in turbulent flow (i.e., a drag law). In their most simple forms for depth-averaged, Reynolds-averaged, steady and uniform condition, these equations for bed friction are

$$\tau_{bd} = \rho g h_R S, \quad (1A)$$

and

$$\tau_b = \rho C_f U^2, \quad (1B)$$

where τ_{bd} is the driving stress acting on the fluid due to gravitational acceleration, τ_b is the shear stress on the bed due to friction, ρ is the fluid density, g is gravitational acceleration, h_R is the hydraulic radius of the flow, S is bed slope, C_f is a friction coefficient (e.g., Chow, 1959), and U is the depth-averaged flow velocity. For the case of steady and uniform flow, $\tau_b = \tau_{bd}$, which is an approximation appropriate for many river systems (e.g., Parker et al., 2007). However, in regions where flow is dynamic in time (e.g., floods) or space (e.g., lateral spreading or confinement), $\tau_b \neq \tau_{bd}$, and spatial and temporal accelerations (excluding turbulent fluctuations) need to be taken into account (e.g., Chow, 1959). Another common assumption is that $h_R = h$, where h is the flow depth, which introduces only a small error (<10%) for channels that are much wider than they are deep ($w > 10h$), a common configuration for most terrestrial alluvial channels. With these assumptions, the hydraulic conservation equations for steady flow can be combined into a single expression for the volumetric flux of fluid in a channel Q,

$$Q = wh\left(\frac{ghS}{C_f}\right)^{1/2}. \quad (2)$$

Thus, assuming that fluid fills a channel of given dimensions (i.e., bankfull flow), the fluid discharge can be calculated from Equation 2 from topographic measurements of channel depth, width, and slope alone, with an appropriate estimate of the coefficient of friction.

The friction coefficient has been found to be a function of the flow Reynolds number (i.e., $\mathrm{Re} = Uh/\nu$, where ν is the kinematic viscosity of the fluid) for laminar flows ($\mathrm{Re} < 500$) and is independent of the fluid viscosity and Re for turbulent flows with hydraulically rough beds (i.e., $\mathrm{Re} > 10^3$ and $\mathrm{Re}_{k_s} > 100$, where $\mathrm{Re}_{k_s} = \frac{u_* k_s}{\nu}$ is the bed roughness Reynolds number, $u_* \equiv \sqrt{\tau_b/\rho}$ is the shear velocity, and k_s is a characteristic bed roughness length scale; Nikuradse, 1933; Schlichting, 1979; Garcia, 2007). On Earth, flow is predominantly turbulent, and this condition likely holds true on Titan as well (Perron et al., 2006), especially for meter-plus–scale channel widths. For example, given that liquid methane has a kinematic viscosity (ν) of 4×10^{-7} m^2 s^{-1} for Titan's surface conditions (http://webbook.nist.gov), flows with a discharge per unit width (Uh) greater than 4×10^{-4} m^2 s^{-1} (i.e., depths of centimeters and velocities of centimeters per second) will be turbulent. Furthermore, hydraulically rough conditions are expected in river channels that transport sediment of diameter $D > 1$ mm over a flat bed. Hydraulically rough conditions may exist for finer sediment if bed forms (e.g., ripples or dunes) or other larger roughness elements are present. For turbulent, hydraulically rough flow conditions, many empirical parameterizations have been proposed for C_f, which depend on the ratio of the flow depth to the bed-roughness length scale. For example, one formula for C_f for gravel-bed rivers is $C_f = (8.1[h/k_s]^{1/6})^{-1/2}$, where $k_s = 2D$ or $3D$ (Parker, 1991). Because C_f is independent of fluid density, viscosity, and gravity for turbulent, hydraulically rough flow conditions, it should be applicable to similar conditions, e.g., gravel-bed rivers, on Titan.

Application to Titan

Formulae like Equation 2 have been used to calculate bankfull flow discharge for putative fluvial channels on Titan (Perron et al., 2006; Jaumann et al., 2008; Lorenz et al., 2008a). Perhaps the biggest limitation in these calculations is the assumption of flow width, because the nature of the fluvial features—whether river channels or river valleys—is uncertain. If this parameter could be determined, however, then we expect these hydraulic formulae to be valid for Titan. In particular, if the flow is fully turbulent and the boundary is rough, then the hydraulics are insensitive to fluid viscosity,

making hydraulics equations developed for Earth directly applicable to Titan conditions when the difference in gravity and fluid density are accounted for in Equations 1A and 2. If the boundaries are hydraulically smooth or the flow Reynolds number is sufficiently low, then the kinematic viscosity of the fluid will need to be known to make quantitative predictions of flow rates.

Sediment Transport

Fluvial networks transport the products of weathering from hillslopes and upstream channels in both the solid and dissolved state. The total sediment flux (or "load") per unit width shown in Equation 1 can be divided into bed load (q_b) and suspended load (q_{sus}), such that $q_s = q_b + q_{sus}$. The dissolved load (q_d) is a volumetric flux and affects the land surface, but it is not part of the sediment flux unless or until it precipitates. In terrestrial landscapes, suspended transport is often the dominant mode, although bed load can dominate in steep, rapidly eroding terrain, and dissolved load may be dominant in karst terrains. Even where bed-load flux is a minor fraction of the total load, bed material dynamics can be important in controlling channel morphology and roughness and in modulating the rate of incision into underlying bedrock.

Incipient Motion

As the motion of fluid in a river imparts a critical shear stress to the riverbed, available sediment typically begins to move as bed load by rolling and bouncing. For a range of sediment sizes and flow conditions, the criterion for entrainment can be calculated from the nondimensional bed shear stress, also known as the Shields stress, defined as

$$\tau_* \equiv \frac{\tau_b}{(\rho_s - \rho) gD}. \quad (3)$$

Shields (1936) showed that the critical value of this stress, τ_{*c}, for incipient motion, varies with the particle Reynolds number, $Re_p = \frac{(rgD)^{1/2} D}{\nu}$, where r is the submerged specific gravity of the sediment ($r = [\rho_s - \rho]/\rho$, where ρ_s and ρ are the densities of sediment and fluid, respectively) for small Re_p and is roughly constant (i.e., $\tau_{*c} \approx 0.045$; Miller et al., 1977; Wilcock, 1993) for $Re_p > 10^2$. The condition for constant critical Shields stress is met for $D > \sim 1$ mm for conditions on both Earth and Titan, taking values for Titan of $r = 1.18$, $g = 1.35$ m/s^2, and $\nu = 4 \times 10^{-7}$ m^2/s for transport of water-ice sediment by flowing methane (e.g., Burr et al., 2006; Perron et al., 2006).

In low-gradient rivers, the increased particle exposure and lower friction angles of larger particles tend to offset the effects of their greater weight, rendering mixtures of different sizes nearly equally mobile (Parker et al., 1982; Wiberg and Smith, 1987; Parker, 1990). Thus, a prediction of incipient motion of the median particle size often is representative of the entire bed. This assumption breaks down, however, in bimodal mixtures, where τ_{*c} can decrease by ~2-fold (Wilcock and Crowe, 2003), and on steep slopes ($S > 1\%$), where τ_{*c} can increase by up to an order of magnitude due to particle emergence (reducing the cross-sectional area exposed to flow) and changes to turbulent mixing in very rough conditions (Lamb et al., 2008c). Expressions that partition bed-load flux among discrete grain-size classes have been developed (e.g., Parker, 1990) and should be used for the cases of bimodal sediment mixtures (Wilcock and Crowe, 2003), which DISR images (Tomasko et al., 2005) suggest may exist on Titan.

Suspension

At larger flow velocities or (for a given channel configuration) lower gravity, sediment motion in suspension, whereby the stream sediment rarely contacts the bed, is enhanced (Komar, 1980). The suspended load is composed both of material entrained from and exchanged with the bed, termed "suspended bed material load," and of the finer particles supplied from upstream that settle too slowly to exchange with the bed, termed "wash load."

Suspension occurs where the fallout under gravity is balanced by entrainment due to turbulence. The conditions for suspended sediment transport can be determined from the bed stress necessary to initiate particle suspension, which be found from

$$\tau_b = \rho w_s^2, \quad (4)$$

where w_s is the particle settling velocity (Bagnold, 1966). Settling velocities may be determined experimentally. Dietrich (1982), for example, explicitly accounted for particle and fluid densities, fluid viscosity, and the acceleration due to gravity, making those formulations directly applicable to Titan conditions. For this approach, particle shape and roundness are required, which are not well known for Titan, but which might be approximated for at least one location from data at the *Huygens* landing site. Empirical data for non-Newtonian flow (Turton and Clark, 1987; Kelessidis, 2004) have been converted into settling velocities for silicate sediment on Earth and for hypothesized organic and water-ice sediments on Titan (Burr et al., 2006). This work assumes spherical particles, which again requires evaluation for Titan.

The transitions between sediment transport modes can be described using the Rouse number, P, which is a ratio of grain settling velocity to turbulence acting to suspend grains and equal to $w_s/\kappa u^*$, where u^* is the shear velocity, and $\kappa = 0.407$ is the von Karman constant. The transition from bed load to suspended load is $P \sim 2.5$ and for suspension to wash load is $P \sim 0.8$. The threshold of bed-load motion has been treated separately, above.

Application to Titan

To apply terrestrial sediment transport equations to Titan, a limited number of parameters need to be adjusted, including gravitational acceleration, the densities of fluid and sediment, and the fluid viscosity. These calculations indicate that both water-ice and organic particles fall through liquid methane on Titan more slowly than do silicate clasts in water on Earth, primarily because of the lower gravity, although this gravitational effect is partly offset by the greater submerged specific gravity (r) of the grain and the lower viscosity (ν) of the liquid (Burr et al., 2006). As a result, for a given grain size, a lower shear velocity is required to drive grain motion across thresholds between transport modes (Fig. 6). A key unknown in estimating sediment transport modes and rates on Titan is the spatial distribution of grain sizes, which depends on the size distribution supplied to the channel network and the rate of particle breakdown in transport. Analysis of the backscatter from radar-bright fluvial features, which implies a cover of rounded ice cobbles (Le Gall et al., 2010), as well as the rounded cobbles at the *Huygens* landing site (Tomasko et al., 2005), suggests that, although rounding during transport may be efficient, breakdown may be limited.

The density of sediment particles in Titan riverbeds may be variable because multiple candidate surface materials could dominate the local supply of sediment particles. Near-surface spectra from the *Huygens* probe are consistent with the presence of water-ice and organic tholin compounds along with an unknown IR-blue material (Schröder and Keller, 2008). Microwave scattering from Titan's surface is also consistent with a mix of fractured or disaggregated water-ice particles and "fluffy" deposits of organic materials (Janssen et al., 2009). The bulk of Titan's crust is likely predominantly composed of water-ice, with a relative density to liquid methane of ~2.1, and this ice may make up a significant fraction of the sediments. The gravel- and cobble-strewn surface at the *Huygens* landing site appears to be more enriched with water-ice particles than the surrounding areas (Keller et al.,

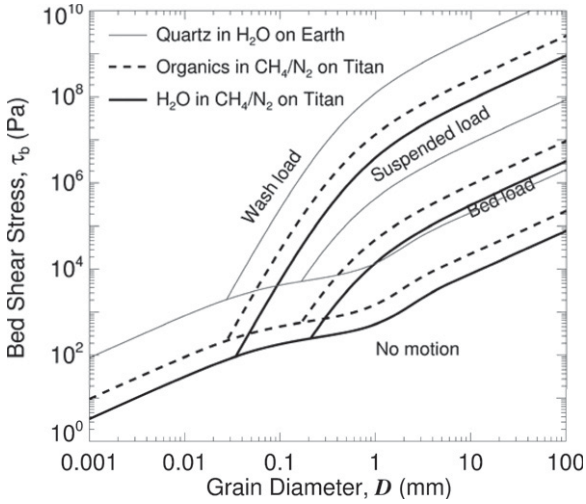

Figure 6. Sediment transport diagram showing the bed shear stress required for each sediment transport mode. For a given grain diameter, lower stress is required for both types of Titan materials than for terrestrial conditions (modified from Burr et al., 2006).

2008). The atmosphere is also a source of fine sediment in the form of micron-sized organic aerosol particles (Waite et al., 2009). Dunes on Titan are likely made of sand-sized organic particles (Barnes et al., 2008) that may have agglomerated over time from these smaller aerosol particles. The density of the organic sediments on Titan is relatively unconstrained—if they are solid, they could be significantly denser than water-ice (e.g., Khare et al., 1994), but if they are porous, they could be less dense than ice. A lack of knowledge regarding the exact types and proportions of the fluvial liquid hydrocarbons on Titan also adds some uncertainty to these results.

Our discussion of sediment transport thresholds assumes that the sediment particles are not cohesive. This assumption may be reasonable for water-ice particles, but for sediments composed of, or covered by solid tholins (Barnes et al., 2008), it may not be correct. The morphology of some terrestrial longitudinal dunes is hypothesized to be the result of the sand particles being slightly cohesive (Rubin and Hesp, 2009). If this hypothesis is correct and applicable to Titan, then organic sediment particles may be less prone to saltate than water-ice particles, and the sediment transport threshold stresses derived for Titan would represent lower limits.

Bedrock Erosion

Under supply-limited conditions, when sediment transport capacity (q_{sc}) exceeds sediment supplied to the river (q_s), bedrock may be exposed in some or all of the channel bed and subject to erosion. Erosion of terrestrial bedrock occurs primarily through abrasion by bed load and suspended load particles ("tools") and by plucking (or "quarrying") of fracture-bounded blocks (Whipple, 2004). Less-common mechanisms include dissolution in carbonate rocks, hydration-fracturing in clay-rich shales, and cavitation on surfaces that protrude into high-velocity flow (Whipple et al., 2000).

Sediment (Tools) Production

On Earth, fluvial sediment production generally requires physical and/or chemical weathering to reduce coherent bedrock to transportable sizes—typically less than meter-scale. On Titan, some sediment may be organic particulates from atmospheric sources (such as the sediment forming the tropical dunes), but this sediment should be fine grained and probably could not facilitate widespread valley incision and formation of steep slopes, as observed in DISR data (Tomasko et al., 2005; Soderblom et al., 2007b). The Titan crust is primarily water-ice with some mixture of other compounds. Recent experimental work, showing the difficulty of eroding coherent icy bedrock, suggests that the bedrock on Titan must be pervasively fractured prior to fluvial erosion (Collins et al., 2011). However, no relevant chemical or physical weathering processes that would pervasively break down coherent ice bedrock have been identified. Meteor impact can reduce rock to transportable sizes, but Titan's observed crater population is sparse (Wood et al., 2008). However, if, Titan did not develop a thick, volatile-cycle–sustaining atmosphere until relatively late in Solar System history (e.g., McKay et al., 1993; Lorenz et al., 1997), then the initial surface could have had a substantial impact-generated regolith layer generated prior to the onset of fluvial activity. Such a starting icy regolith could have provided ample tools for incision and/or sediment for transport once the rains began.

Incision Rates and Mechanisms

The rate of fluvial incision is conventionally assumed to follow power-law scaling with some metric of flow intensity, such as average bed shear stress (τ_b) or stream power per unit bed area (ω). The empirical coefficients in these relationships are complex parameters into which many variables are lumped, including the rock resistance to erosion, channel roughness and geometry, the efficiency of the dominant erosional processes, and the inherent tradeoffs between the magnitude and frequency of discharges capable of eroding bedrock (Howard and Kerby, 1983; Whipple and Tucker, 1999). This scaling approach is appealing because of its simplicity, and it is readily incorporated into landscape evolution models. Using hydraulic conservation equations (e.g., Eq. 2), and assuming that flow depth and discharge (for a given flood recurrence interval) can be expressed as functions of drainage area (A), the incision rate can be written as

$$E = kA^m S^n, \quad (5)$$

where the parameters k, m, and n are model-specific parameters empirically calibrated using river longitudinal profiles that are assumed to be in topographic steady state or where initial and boundary conditions are known (Whipple, 2004).

This stream power approach is of limited utility for simulating rates of channel incision on Titan because of the lack of physical constraints on the model parameters under Titan conditions. Process-specific models, ideally with physically explicit parameters, are better suited to exploring controls on rates and patterns of landscape evolution. However, without information about hydraulic geometry and the frequency and magnitude of flows, even erosion models with physically explicit parameters will be of limited utility for modeling absolute rates of landscape evolution.

Brief discussion of specific erosion processes shows the present extent of applicability of these process-specific models to Titan. Plucking is the removal of material from a channel bed "by lifting or sliding of blocks defined by an existing set of discontinuities in the rock" (Hancock et al., 1998), and it results from pressure fluctuations in highly turbulent flows. It can be modeled as a power function of bed shear stress (τ_b) in excess of the threshold stress (τ_c) required to initiate detachment (e.g., Whipple et al., 2000):

$$E = k\left(\tau_b - \tau_c\right)^n, \quad (6)$$

where k and n are model-specific parameters. More physically explicit models are available for bedrock wear by abrasion by saltating bed load (Sklar and Dietrich, 2004) and by bed load and suspended load particle impacts (Lamb et al., 2008b). These models are based on the

notion that sediment provides abrasive tools, but at high supply rates, transient sediment deposits can cover and protect underlying bedrock from all erosive mechanisms except dissolution. A general expression that encompasses tools and cover, as well as most other published incision model formulations (Sklar and Dietrich, 2006), can be written as

$$E = k\left(\gamma - \gamma_c\right)^a q_s^b \left(1 - \frac{q_s}{q_{sc}}\right)^c, \qquad (7)$$

where k is model specific, γ is a generic flow intensity variable (e.g., shear stress, Shields stress, stream power, etc.), γ_c is the value of γ at the onset of sediment motion or bedrock detachment depending on model assumptions, q_s and q_{sc} are the sediment supply (flux) and transport capacity per unit width, respectively, and the empirical exponents b and c control the tools and cover effects, respectively. For wear by particle impacts, rock resistance varies with the square of tensile strength (Sklar and Dietrich, 2001). However, for other incision mechanisms, little is known about the ways in which wear rates scale with rock material properties (Whipple, 2004). To apply a tools-and-cover model as shown in Equation 7, predictive relations are needed for the spatial variation in grain size and supply rate of sediment delivered to channel networks by hillslopes. In terrestrial models, sediment supply is often estimated as the product of drainage area and long-term mean denudation rate, and partitioned arbitrarily between coarse bed load and finer suspended load (e.g., Sklar and Dietrich, 2006). At present, little is known about the controls on grain-size distribution of sediments supplied to channels on Earth (Attal and Lavé, 2006) or on Titan.

Another set of bedrock incision mechanisms is associated with migrating knickpoints and waterfalls, including plunge pool scour, undercutting, seepage, and block toppling (Lamb et al., 2006; Lamb and Dietrich, 2009), as well as effects on upstream channels due to flow acceleration approaching free fall (Haviv et al., 2006). Debris flows can also be important agents of channel incision in headwater channels (Stock and Dietrich, 2006), where steep slopes tend to generate sediment flows. However, global relief on Titan is lower than on Earth (Perron and de Pater, 2004; Jaumann et al., 2009; Lorenz et al., 2011), which may serve to reduce the geomorphic effectiveness of debris flows, if all other factors are assumed to be equal.

Application to Titan

Scaling terrestrial bedrock incision models to Titan is difficult due to the uncertainty as to which erosional processes are dominant and to the weak physical basis for most terrestrial model formulations. Abrasion by ice clasts (Collins, 2005) moving as bed load and/or suspended load (Burr et al., 2006) is a reasonable candidate mechanism, given the rounded grains observed at the *Huygens* landing site (Tomasko et al., 2005). This process can be modeled with physically explicit sediment-abrasion models (Sklar and Dietrich, 2004; Lamb et al., 2008b). Parameters that need to be adjusted for Titan conditions include gravity, the buoyant density of sediments, and possibly the fluid viscosity for modeling wear by finer-grained suspended particles, depending on the particle Reynolds number. Incision rates predicted by the saltation-abrasion model, for fixed channel geometry and sediment conditions, are remarkably similar for Earth and Titan (Collins, 2005), as Titan's lower gravity and higher sediment buoyancy are partially offset by lower resistance to impact wear for water-ice compared to rock of similar tensile strength (Polito et al., 2009).

The material properties of ice bedrock and regolith on Titan are first-order controls on the occurrence and efficiency of the various possible incision mechanisms. The tensile strength and erosion resistance of polycrystalline water-ice increases with decreasing temperature (Polito et al., 2009; Litwin et al., 2012), and the strength is sensitive to ice grain size and porosity (Schulson and Duval, 2009). Moreover, ice erodibility may be influenced by impurities such as atmospherically derived tholins (e.g., Soderblom et al., 2007a) and cryovolcanically derived ammonium sulfate compounds (Fortes et al., 2007), although evidence for cryovolcanism on Titan has been challenged (Moore and Pappalardo, 2011). The extent and characteristic scale of fracturing in ice bedrock will influence the grain size supplied to channels, as well as the potential role of plucking and knickpoint retreat in channel incision. Whether landslides and debris flows occur on Titan depends in part on the extent of disaggregation of hillslope bedrock and on the dynamics of methane rainfall infiltration and runoff.

Bed Morphology

Channel bed morphology is important for fluvial processes and landscape evolution because of its influence on hydraulic roughness, sediment transport and erosion rates, and the dominant bedrock incision mechanisms (Wohl, 2000). Bed morphology varies systematically through terrestrial river networks and is strongly influenced by bed material grain size. The influence of flow hydraulics on bed configuration is better understood mechanistically for low-gradient, sand-bedded channels on Earth. Only conceptual models and rough empirical correlations are available for steeper, gravel- and coarser-bedded terrestrial channels (Montgomery and Buffington, 1997).

Low-Gradient Terrestrial Channels

In relatively low-gradient channels on Earth, a predictable sequence of bed morphologies develops with increasing bed shear stress, including ripples, upper plane bed, and antidunes for beds of silt and fine sand, and lower plane bed, dunes, upper plane bed, and antidunes for beds of coarse sand and gravel (e.g., Southard, 1991). In steady, uniform, open-channel flow of a Newtonian fluid, dimensional analysis indicates that at least three key dimensionless variables are needed to describe stable bed-form states (Vanoni, 1974; van Rijn, 1984; Southard, 1991; van den Berg and van Gelder, 1993). These dimensionless variables provide a set of scale-modeling parameters that can take into account a wide range of sedimentologically interesting behaviors such as the effects of changing grain size, current velocity, flow depth, fluid viscosity, grain density, and the acceleration of gravity. Herein, we describe bed states by representing the flow strength (or intensity of sediment transport) through the dimensionless Shields stress, τ_* (Eq. 3), and the effective sediment size using the particle Reynolds number, Re_p, along with the Froude Number, $Fr = \frac{U}{\sqrt{gh}}$, as the final dimensionless number needed to describe bed-form stability in this framework. Numerous flume experiments have shown that for Fr >~1, flows are considered supercritical, and antidunes form rather than ripples, dunes, or plane beds (Vanoni, 1974; van Rijn, 1984; Southard and Boguchwal, 1990a). For Fr <1, bed-form stability is independent of Fr and therefore can be neglected as a variable for the analysis of ripple bed forms of concern here (van den Berg and van Gelder, 1993).

We have compiled results from five sediment transport and bed-form studies to build a comprehensive bed-form stability diagram for $Fr < 1$ that spans a large range in Re_p (Fig. 7A) (Chabert and Chauvin, 1963; White, 1970; Brownlie, 1983; Southard and Boguchwal, 1990b; van den Berg and van Gelder, 1993). Each study contains many data points (in cases thousands) that each represent a single flume experiment or field observation, and these data points are not reproduced here. Instead, the dividing lines were found empirically to bound the bed-form stability fields from each study, with solid lines where the stability fields have been explored experimentally or with field data, and dashed lines where data represent power-law extrapolations (Fig. 7A). For the case of Southard and

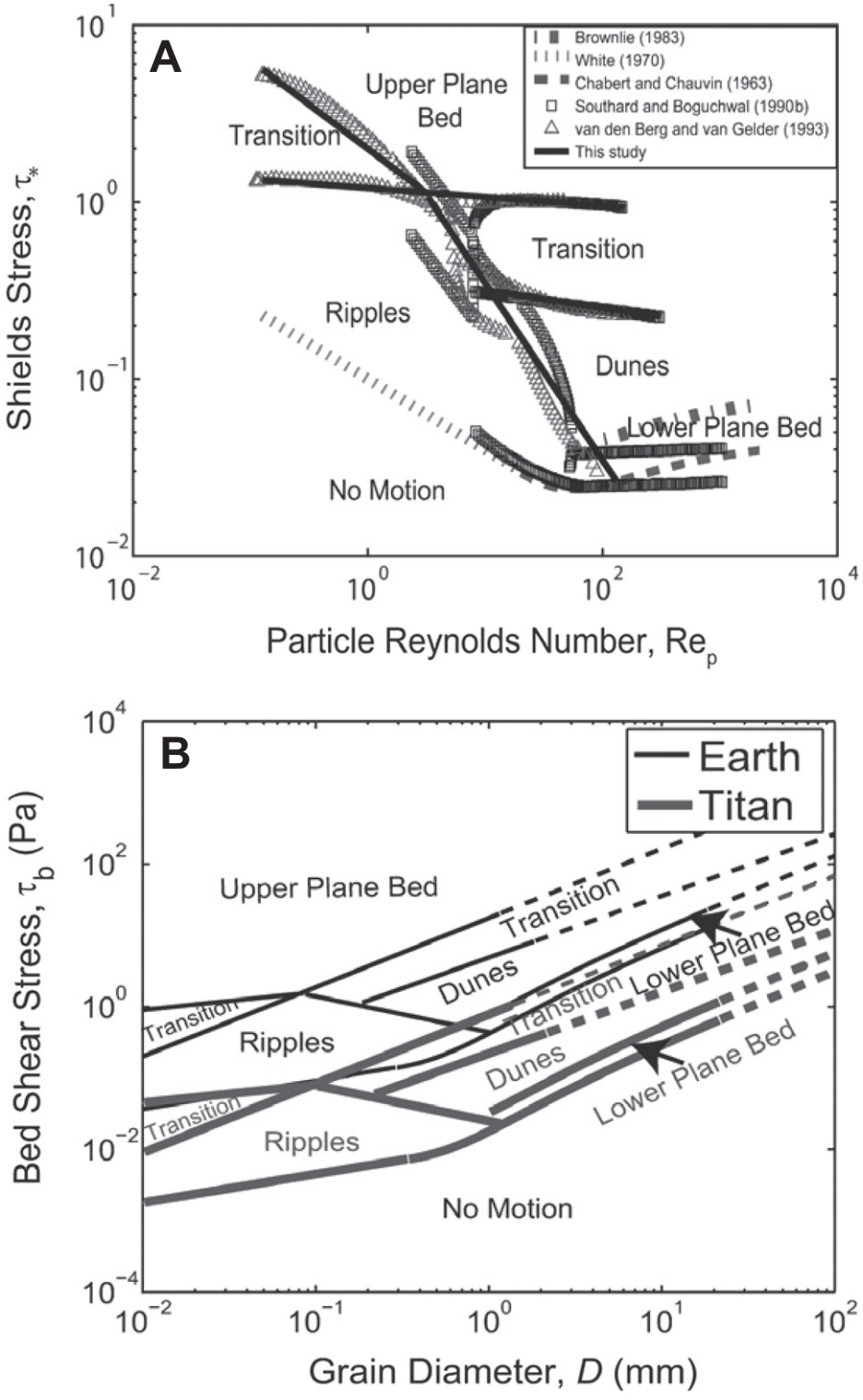

Figure 7. Bed-form stability diagrams for low-gradient rivers. (A) Nondimensional representation of stable bed forms. Solid lines are boundaries between bed states that have been explored based on five previous studies and compilations (Chabert and Chauvin, 1963; White, 1970; Brownlie, 1983; Southard and Boguchwal, 1990b; van den Berg and van Gelder, 1993). (B) Dimensional representation of stable bed states for methane flows transporting water-ice particles on Titan (thick lines), and freshwater flows transporting siliceous material on Earth (thin lines). Dashed lines are power-law extrapolations of stability boundaries from part A. "Upper plane bed" and "lower plane bed" apply to both Titan and Earth conditions.

Boguchwal (1990b), we recast their dimensional diagram (their fig. 11) into the dimensionless variables τ_* and Re_p. The compilation shows a lower boundary separating no motion from the fields of sediment transport, i.e., the Shields curve (Shields, 1936). In the regimes of mobile sediment, ripples form at low Re_p and moderate values of τ_*, and ripples begin to wash out to upper plane bed at $\tau_* > \sim 1$. For large Re_p, a stable regime of lower plane bed is followed with increasing Shields parameter by dunes and upper plane bed. The results are robust even though the databases contain field data, flume data, and measurements made by different authors, and even though they span a wide range of flow velocities, flow depths, particle sizes, particle densities, fluid densities, and fluid viscosities.

Application to Titan

The bed-form stability diagram reveals that stable bed-form states depend on fluid and particle density, viscosity, and gravity, all of which are different for flows on Titan as compared to Earth. To illustrate this effect, we replot the stability fields in terms of the flow stress on the bed (τ_b) versus particle diameter (D) (Fig. 7B). This replotting requires values for the physical properties of the flows and sediment on Titan, approximated as $r = 1.18$, $\nu = 4 \times 10^{-7}$ m^2/s, and $g = 1.35$ m/s^2 for transport of water-ice sediment by flowing methane. A reference case for freshwater flows on Earth is also shown with $r = 1.65$, $\nu = 10^{-6}$ m^2/s, and $g = 9.81$ m/s^2.

This dimensional plot shows a significant shift in bed-form stability for conditions on Titan as compared to Earth (Fig. 7B), primarily due to the 10-fold reduction in the submerged specific weight of the sediment (i.e., rg). For example, sediment of size $D = 0.1$ mm on Titan is predicted to have an upper plane bed configuration, the highest energy state, for the same bed stresses at which the same size sediment is at the threshold of motion on Earth. Despite the drastic change in fluid stresses for Titan conditions, the equivalent bed forms are expected to form in the same sediment sizes on Titan as on Earth. For example, ripples are expected for $D < \sim 0.1$ mm and dunes for $D > \sim 2$ mm, with both bed forms possible for intermediate sizes, whether on Earth or Titan. This similarity of bed forms with sediment size is because the lower fluid viscosity on Titan by a factor of 2.5 is compensated for by the decrease in submerged specific weight of the sediment in the calculation of Re_p.

High-Gradient Terrestrial Channels

Upstream of the gravel-sand transition, terrestrial riverbeds display a predictable sequence of channel types correlated strongly with slope

(*S*), progressing downstream from cascade to step-pool to alternating bar-pool morphology, as drainage area, channel width, sediment supply, discharge, and mean flow velocity all increase and grain size systematically decreases (Montgomery and Buffington, 1997; Knighton, 1998). These characteristic trends result from downstream shifts in the dominant processes delivering sediments (e.g., debris flows to bank erosion), and the scale and type of hydraulic roughness elements (e.g., boulders to bars), as well as the increase in width-depth ratio and the shift from confined to floodplain valley bottoms (Montgomery and Buffington, 1997). Hillslope sediment production and delivery processes and valley-bottom morphology largely control coarse-bedded channel morphologies, but because we currently lack a nondimensional framework for these processes, they cannot yet be scaled to Titan.

SUMMARY AND AREAS FOR FUTURE INVESTIGATION

Here, we summarize our main findings, and we suggest some areas for future investigations.

(1) At the landscape scale, Titan fluvial networks imaged in SAR data include rectangular, dendritic, and parallel morphologies (Burr et al., 2009b; Drummond et al., 2012). In this analysis to date, rectangular networks are inferred to predominate, although current SAR resolution limits our ability to distinguish rectangular from trellis networks (Drummond, 2012). Higher-resolution data, as from an airplane (Barnes et al., 2012), would improve our network classification. Either rectangular networks or trellis networks imply structural control on runoff, and analysis of the predominant azimuths would provide information on the hypothesized controlling structures.

(2) At the reach scale, varied morphologies (Table 1) imply a range of fluvial processes (Table 1). In general, data do not support interpretation of these features as single-thread channels, but as river valleys, braid plains, anabranching channels, or other features for which direct discharge estimation based on morphology (feature width) is invalid. These interpretations can be tested by global mapping of fluvial feature morphology in comparison with geologic context, terrain type, local and regional relief, composition, and other parameters. Comparison of morphometric data from Titan and terrestrial fluvial landscapes would provide another test. For example, channel widths implied by the interpretation of either the Huygens or Cassini features as channels may be significantly out of proportion to typical channel width–drainage area relations on Earth (Knighton, 1998). However, terrestrial relations, being empirical, may scale differently on Titan.

(3) If some features are inferred to be channels, then questions may be raised pertaining to meandering (e.g., Fig. 2C). Meandering channels require some bank material cohesion, which on Earth is associated with plants (Davies and Gibling, 2010a; Davies and Gibling, 2010b). However, meandering paleochannels are also inferred for Mars (Malin and Edgett, 2003; Moore et al., 2003; Burr et al., 2009a, 2010). If some sinuous fluvial features on Titan are determined to be meandering river channels (as opposed to river valleys), then they would imply a second example of a nonbiological cohesion mechanism. Cohesion has been suggested for the material at the Huygens landing site (Atkinson et al., 2010). Laboratory investigation of the properties of Titan sediments would contribute to addressing this question.

(4) The morphology of valley networks observed near the *Huygens* landing site is most consistent with mechanical erosion by channelized flows fed by atmospheric precipitation, though sapping erosion is a possibility if the surface material is cohesionless. Laboratory investigations into cohesion, permeability, and other properties of Titan analog sediments would contribute to addressing this issue.

(5) Comparison of DISR and SAR images suggests that highlands elsewhere on Titan are dissected by fluvial features at scales finer than the resolution of SAR data. We hypothesize that extensive fine-scale dissection exists within crenulated terrain (e.g., Fig. 2F), in which case dissection of Titan's surface may be much more extensive than can be inferred from resolved networks. This hypothesis may be tested by textural analysis of Titan SAR images for comparison with SAR images of fluvially and nonfluvially dissected terrain on Earth.

(6) The incised appearance of some fluvial features implies the existence of sediment that acts as erosive tools. In addition, sites of fluvial sediment deposition are inferred from SAR data to include braid plains, fan-shaped deposits, and lake basins, and DISR images at the surface show rounded sediment of sizes that could reasonably be moved by channelized flow. However, the mechanism for generating such fluvial sediment on Titan is uncertain. Additional laboratory experiments would contribute to understanding incision into Titan bedrock, and more refined mapping of Titan's surface may indicate (a) source(s) for the erosive sediments.

(7) Observations and modeling show that fluvial runoff on Titan can be supplied by precipitation, which may follow a variety of flow paths to the fluvial networks. Additional information about surface material properties on Titan, e.g., porosity and permeability, stratification, and solubility, would contribute to inferences about the locations, timing, and efficiency of each flow path. Estimations of the amount of runoff and the recurrence interval of the channel-forming (dominant) discharge require additional information on precipitation patterns and mechanical properties of the surface.

(8) Channelized flow may be modeled using terrestrial hydraulic formulae with appropriate modifications. If the flow is fully turbulent and the boundary is rough, then hydraulic equations developed for Earth are directly applicable to Titan conditions with changes in gravity and fluid density. If the boundaries are hydraulically smooth or the flow Reynolds number is sufficiently low, then knowledge of the kinematic viscosity of the fluid is necessary, which requires knowing the behavior of particles of appropriate size and composition in liquid hydrocarbons.

(9) Sediment transport on Titan may be defined using stability fields. For model sediment densities and equivalent flow conditions, transport requires less shear stress on Titan than on Earth for equivalent grain size. However, the geomorphic effect of this lower shear stress depends on the alkanology, including the frequency of flows that exceed the transport threshold. Rainfall and infiltration rates and locations are fundamental inputs into the rates, locations, and types of overland and near-surface flow, which in turn control the river flow regimes, sediment transport, and incision that shape the landscape. Sediment production rate, the flux of sediment from hillslopes into stream channels, and the sorting and breakdown effects of fluvial processes on sediment would provide important information for interpreting the fluvial and global sediment cycle on Titan. One distinctive aspect of fluvial processes on Titan is the continuous deposition of aerosols onto the surface and their apparent removal from higher-relief surfaces. Constraining this rate of aerosol deposition and removal is vital for accurate fluvial sediment transport modeling.

(10) Under supply-limited conditions, bedrock may be exposed in the channel. Bedrock incision rates under Titan conditions could be derived with knowledge of model parameters for specific processes (e.g., plucking, abrasion, knickpoint retreat), but this knowledge is currently unavailable. Ongoing investigations into icy bedrock tensile strength indicate that preconditioning of water-ice is important for creation of icy fluvial sediment on Titan (Collins et al., 2011; Litwin et al., 2012). However, mechanisms for pervasive breakdown of bedrock remain uncertain.

(11) Scaling the mechanics of low-gradient sand beds to Titan shows that bed morpholo-

gies are stable at significantly lower stresses than they are under terrestrial conditions. However, the factors controlling the morphology of steeper, gravel-bed channels on Earth are not sufficiently understood to allow such scaling.

ACKNOWLEDGMENTS

Support for Burr, Irwin, Perron, Drummond, and Black was provided by a *Cassini* Data Analysis Program grant to Burr. Collins and Sklar were supported by an Outer Planets Research Program grant to Collins. Moore and Howard were supported by an Outer Planets Research Program grant to Moore. We acknowledge support from the University of Tennessee Exhibit, Performance, and Publication Expense Fund. We thank Tom Farr for processing the synthetic aperture radar (SAR) images in Figure 4. We gratefully acknowledge Trent Hare for his Titan ArcGIS project and Randy Kirk and Alex Hayes for helpful information. We thank the editors for their assistance in helping us shape this publication appropriately, and Bob Craddock, Ralph Lorenz, and an anonymous reviewer for providing useful comments. Most of all, we thank the *Cassini* and *Huygens* spacecraft mission teams for their successful efforts to produce the data used in this manuscript.

APPENDIX

Symbology

Variable	Dimensions	Description
A	L^2	drainage area
C_0		suspended load concentration at a reference bed elevation z_0
C_f		friction coefficient
C_s		volumetric concentration of suspended sediment
D	L	sediment grain diameter
E	L/T	rate of channel-bed lowering for bedrock rivers
g	L/T^2	gravitational acceleration
h	L	depth of flow
h_R	L	hydraulic radius
K		dimensionless coefficient for bed-load flux models
k, n		empirically calibrated parameters for incision models
k_s	L	characteristic bed roughness length scale
P		Rouse number
Q	L^3/T	volumetric flux of fluid
q_b	L^2/T	volumetric flux of bed load per unit channel width
q_{bc}	L^2/T	volumetric bed-load transport capacity per unit channel width
q_d	L^2/T	volumetric flux of dissolved load per unit channel width
q_s	L^2/T	volumetric flux of sediment per unit channel width
q_{sc}	L^2/T	volumetric sediment transport capacity of a flow per unit channel width
q_{sus}	L^2/T	volumetric flux of suspended load per unit channel width
r		specific density of sediment submerged in fluid
S		channel-bed slope
U	L/T	depth-averaged flow velocity
u_*	L/T	shear velocity
w	L	width of flow
w_s	L/T	particle settling velocity
z	L	height above bed within flow
z_0	L	a reference bed elevation at base of the profile
α		ratio of eddy viscosity for momentum to eddy diffusivity for sediment
γ		Generic flow intensity variable (Eq. 9)
γ_c		Critical value of generic flow intensity variable (Eq. 9)
κ		von Karman constant
ν	L^2/T	kinematic viscosity of fluid
ρ	M/L^3	fluid density
ρ_s	M/L^3	sediment density
τ_b	$M/L/T^2$	fluid shear stress acting on the bed
τ_{bd}	$M/L/T^2$	gravitational driving stress acting on the fluid
τ_c	$M/L/T^2$	threshold bed shear stress to initiate detachment
τ_*		Shields stress
τ_{*c}		critical Shields stress
ω	M/T^3	stream power per unit bed area

REFERENCES CITED

Ádámkovics, M., Wong, M.H., Laver, C., and de Pater, I., 2007, Widespread morning drizzle on Titan: Science, v. 318, no. 5852, p. 962–965, doi:10.1126/science.1146244.

Ádámkovics, M., de Pater, I., Hartung, M., and Barnes, J.W., 2009, Evidence for condensed-phase methane enhancement over Xanadu on Titan: Planetary and Space Science, v. 57, no. 13, p. 1586–1595, doi:10.1016/j.pss.2009.07.001.

Ádámkovics, M., Barnes, J.W., Hartung, M., and de Pater, I., 2010, Observations of a stationary mid-latitude cloud system on Titan: Icarus, v. 208, no. 2, p. 868–877, doi:10.1016/j.icarus.2010.03.006.

Atkinson, K.R., Zarnecki, J.C., Towner, M.C., Ringrose, T.J., Hagermann, A., Ball, A.J., Leese, M.R., Kargl, G., Paton, M.D., Lorenz, R.D., and Green, S.F., 2010, Penetrometry of granular and moist planetary surface materials: Application to the *Huygens* landing site on Titan: Icarus, v. 210, no. 2, p. 843–851, doi:10.1016/j.icarus.2010.07.019.

Attal, M., and Lavé, J., 2006, Changes of bedload characteristics along the Marsyandi River (central Nepal): Implications for understanding hillslope sediment supply, sediment load evolution along fluvial networks, and denudation in active orogenic belts, *in* Willett, S.D., Hovius, N., Brandon, M.T., and Fisher, D.M., eds., Tectonics, Climate, and Landscape Evolution: Geological Society of America Special Paper 398, Penrose Conference Series, p. 143–171, doi:10.1130/2006.2398(09).

Bagnold, R.A., 1966, An Approach to the Sediment Transport Problem from General Physics: U.S. Geological Survey Geological Survey Professional Paper 422-I, 37 p.

Baker, V.R., 1977, Stream-channel response to floods, with examples from central Texas: Geological Society of America Bulletin, v. 88, no. 8, p. 1057–1071, doi:10.1130/0016-7606(1977)88<1057:SRTFWE>2.0.CO;2.

Barnes, J.W., Brown, R.H., Soderblom, L., Buratti, B.J., Sotin, C., Rodriguez, S., Le Mouèlic, S., Baines, K.H., Clark, R., and Nicholson, P., 2007a, Global-scale surface spectral variations on Titan seen from *Cassini*/VIMS: Icarus, v. 186, no. 1, p. 242–258, doi:10.1016/j.icarus.2006.08.021.

Barnes, J.W., and 18 others, 2007b, Near-infrared spectral mapping of Titan's mountains and channels: Journal of Geophysical Research–Planets, v. 112, E11006, doi:10.1029/2007JE002932.

Barnes, J.W., and 12 others, 2008, Spectroscopy, morphometry, and photoclinometry of Titan's dunefields from *Cassini*/VIMS: Icarus, v. 195, no. 1, p. 400–414, doi:10.1016/j.icarus.2007.12.006.

Barnes, J.W., and 30 others, 2012, AVIATR—Aerial Vehicle for In-situ and Airborne Titan Reconnaissance: Experimental Astronomy, v. 33, no. 1, p. 55–127, doi:10.1007/s10686-011-9275-9.

Barth, E.L., 2010, Cloud formation along mountain ridges on Titan: Planetary and Space Science, v. 58, no. 13, p. 1740–1747, doi:10.1016/j.pss.2010.07.013.

Barth, E.L., and Rafkin, S.C.R., 2007, TRAMS: A new dynamic cloud model for Titan's methane clouds: Geophysical Research Letters, v. 34, L03203, doi:10.1029/2006GL028652.

Barth, E.L., and Rafkin, S.C.R., 2010, Convective cloud heights as a diagnostic for methane environment on Titan: Icarus, v. 206, no. 2, p. 467–484, doi:10.1016/j.icarus.2009.01.032.

Barth, E.L., and Toon, O.B., 2006, Methane, ethane, and mixed clouds in Titan's atmosphere: Properties derived from microphysical modeling: Icarus, v. 182, no. 1, p. 230–250, doi:10.1016/j.icarus.2005.12.017.

Baugh, N.F., 2008, Fluvial Channels on Titan [Ph.D. thesis]: Tucson, Arizona, University of Arizona, 45 p.

Beven, K., and Wood, E. F., 1993, Flow routing and the hydrological response of channel networks, *in* Bevin, K., and Kirkby, M.J., eds., Channel Network Hydrology: New York, John Wiley, p. 99–128.

Black, B.A., Perron, J.T., Burr, D.M., and Drummond, S.A., 2012, Estimating erosional exhumation on Titan from drainage network morphology: Journal of Geophysical Research, v. 117, E08006, doi:10.1029/2012JE004085.

Blair, T.C., and McPherson, J.G., 1994, Alluvial fans and their natural distinction from rivers based on morphology, hydraulic processes, sedimentary processes, and facies assemblages: Journal of Sedimentary Research, v. A64, no. 3, p. 450–489.

Bourgeois, O., Lopez, T., Le Mouélic, S., Fleurant, C., Tobie, G., Le Corre, L., Le Deit, L., Sotin, C., and Bodeur, Y., 2008, A surface dissolution/precipitation model for the development of lakes on Titan, based on an arid terrestrial analogue: The pans and calcretes of Etosha (Nambia): Proceedings of the Lunar and Planetary Science Conference XXXIX: Houston, Texas, Lunar and Planetary Institute, Abstract 1733.

Bridge, J.S., and Lunt, I.A., 2006, Depositional models of braided rivers, *in* Sambrook Smith, G.H., Best, J.L., Bristow, C.S., and Petts, G.E., eds., Braided Rivers: Process, Deposits, Ecology, and Management: Oxford, UK, Blackwell Publishing, p. 11–50.

Brown, M.E., Bouchez, A.H., and Griffith, C.A., 2002, Direct detection of variable tropospheric clouds near Titan's south pole: Nature, v. 420, no. 6917, p. 795–797, doi: 10.1038/nature01302.

Brown, M.E., Smith, A.L., Chen, C., and Ádámkovics, M., 2009, Discovery of fog at the south pole of Titan: The Astrophysical Journal, v. 706, p. L110–L113, doi: 10.1088/0004-637X/706/1/L110.

Brown, M.E., Roberts, J.E., and Schaller, E.L., 2010, Clouds on Titan during the *Cassini* prime mission: A complete analysis of the VIMS data: Icarus, v. 205, no. 2, p. 571–580, doi:10.1016/j.icarus.2009.08.024.

Brown, R.H., and 21 others, 2004, The *Cassini* Visual and Infrared Mapping Spectrometer (VIMS) investigation: Space Science Reviews, v. 115, p. 111–168, doi: 10.1007/s11214-004-1453-x.

Brown, R.H., Soderblom, L.A., Soderblom, J.M., Clark, R.N., Jaumann, R., Barnes, J.W., Sotin, C., Buratti, B., Baines, K.H., and Nicholson, P.D., 2008, The identification of liquid ethane in Titan's Ontario Lacus: Nature, v. 454, no. 7204, p. 607–610, doi:10.1038 /nature07100.

Brownlie, W.R., 1983, Flow depth in sand-bed channels: Journal of Hydraulic Engineering, v. 109, no. 7, p. 959–990, doi:10.1061/(ASCE)0733-9429(1983)109:7(959).

Burr, D.M., Emery, J.P., Lorenz, R.D., Collins, G.C., and Carling, P.A., 2006, Sediment transport by liquid surficial flow: Application to Titan: Icarus, v. 181, p. 235–242, doi:10.1016/j.icarus.2005.11.012.

Burr, D.M., Enga, M.-T., Williams, R.M.E., Zimbelman, J.R., Howard, A.D., and Brennand, T.A., 2009a, Pervasive aqueous paleoflow features in the Aeolis/Zephyria Plana region, Mars: Icarus, v. 200, p. 52–76, doi:10.1016/j.icarus.2008.10.014.

Burr, D.M., Jacobsen, R.E., Roth, D.L., Phillips, C.B., Mitchell, K.L., and Viola, D., 2009b, Fluvial network analysis on Titan: Evidence for subsurface structures and west-to-east wind flow, southwestern Xanadu: Geophysical Research Letters, v. 36, no. 22, doi:10.1029/2009GL040909.

Burr, D.M., Williams, R.M.E., Wendell, K.D., Chojnacki, M., and Emery, J.P., 2010, Inverted fluvial features in the Aeolis/Zephyria Plana region, Mars: Formation mechanism and initial paleodischarge estimates: Journal of Geophysical Research, v. 115, E07011, doi:07010.01029/02009JE003496.

Cartwright, R., Clayton, J.A., and Kirk, R.L., 2011, Channel morphometry, sediment transport, and implications for tectonic activity and surficial ages of Titan basins: Icarus, v. 214, no. 2, p. 561–570, doi:10.1016 /j.icarus.2011.03.011.

Chabert, J., and Chauvin, J.L., 1963, Formation des Dunes et des Rides dans les Modeles Fluviaux: Bulletin du Centre de Recherche et d'Essais de Chatou, v. 4, p. 31–51.

Chow, V.T., 1959, Open Channel Hydraulics: New York, McGraw Hill, 680 p.

Collins, G.C., 2005, Relative rates of fluvial bedrock incision on Titan and Earth: Geophysical Research Letters, v. 32, L22202, doi:10.1029/2005GL024551.

Collins, G.C., Polito, P., Litwin, K.L., and Sklar, L.S., 2011, Resistance of water ice to fluvial abrasion and implications for erosion on Titan: Proceedings of the Lunar and Planetary Science Conference 42: Woodlands, Texas, Lunar and Planetary Institute, Abstract 2781.

Coustenis, A., and Taylor, F.W., 2008, Titan: Exploring an Earthlike World: Singapore, World Scientific, 393 p.

Crayosky, T.W., DeWalle, D.R., Seybert, T.A., and Johnson, T.E., 1999, Channel precipitation dynamics in a forested Pennsylvania headwater catchment (USA): Hydrological Processes, v. 13, p. 1303–1314.

Davies, N.S., and Gibling, M.R., 2010a, Cambrian to Devonian evolution of alluvial systems: The sedimentological impact of the earliest land plants: Earth-Science Reviews, v. 98, no. 3–4, p. 171–200, doi:10.1016 /j.earscirev.2009.11.002.

Davies, N.S., and Gibling, M.R., 2010b, Paleozoic vegetation and the Siluro-Devonian rise of fluvial lateral accretion sets: Geology, v. 38, no. 1, p. 51–54, doi:10.1130 /G30443.1.

Dietrich, W.E., 1982, Settling velocity of natural particles: Water Resources Research, v. 18, no. 6, p. 1615–1626, doi:10.1029/WR018i006p01615.

Dingman, S.L., 1970, Hydrology of the Glenn Creek Watershed, Tanana River Drainage, Central Alaska: Research Report 297: Hanover, New Hampshire, USA CRREL, 111 p.

Dingman, S.L., 2002, Physical Hydrology: Upper Saddle River, New Jersey, Prentice Hall, 646 p.

Drummond, S.A., 2012, Structural control of Fluvial Network Morphology on Titan [Master's thesis]: Knoxville, Tennessee, University of Tennessee, 86 p.

Drummond, S.A., Burr, D.M., Cartwright, R., Black, B.A., and Perron, J.T., 2012, Morphologic classification and geologic implications of Titan fluvial features: Proceedings of the 43rd Lunar and Planetary Science Conference: Houston, Texas, Lunar and Planetary Institute, Abstract 2868.

Dunne, T., and Black, R.D., 1970, Partial area contributions to storm runoff in a small New England watershed: Water Resources Research, v. 6, p. 1296–1311, doi:10.1029/WR006i005p01296.

Dunne, T., and Black, R.D., 1980, Formation and controls of channel networks: Progress in Physical Geography, v. 4, no. 2, p. 211, doi:10.1177/030913338000400204.

Dury, G.H., 1964, Principles of Underfit Streams: U.S. Geological Survey Professional Paper 452-A, 67 p.

Dury, G.H., 1985, Attainable standards of accuracy in the retrodiction of palaeodischarge from channel dimensions: Earth Surface Processes and Landforms, v. 10, p. 205–213, doi:10.1002/esp.3290100303.

Elachi, C., and 21 others, 2004, Radar: The *Cassini* Titan Radar Mapper: Space Science Reviews, v. 115, p. 71–110, doi:10.1007/s11214-004-1438-9.

Elachi, C., and 34 others, 2005, *Cassini* Radar views the surface of Titan: Science, v. 308, p. 970–974, doi:10.1126 /science.1109919.

Elachi, C., and 34 others, 2006, Titan Radar Mapper observations from *Cassini*'s T3 fly-by: Nature, v. 441, no. 7094, p. 709–713, doi:10.1038/nature04786.

Farr, T.G., and 17 others, 2007, The Shuttle Radar Topography Mission: Reviews of Geophysics, v. 45, no. 2, RG2004, doi:10.1029/2005RG000183.

Flasar, F.M., Samuelson, R.E., and Conrath, B.J., 1981, Titan's atmosphere: Temperature and dynamics: Nature, v. 292, no. 5825, p. 693–698, doi:10.1038 /292693a0.

Fortes, A.D., Grindrod, P.M., Trickett, S.K., and Vocadlo, L., 2007, Ammonium sulfate on Titan: Possible origin and role in cryovolcanism: Icarus, v. 188, no. 1, p. 139–153, doi:10.1016/j.icarus.2006.11.002.

Gao, B.-C., Chan, P.K., and Li, R.-R., 2004, A global water vapor data set obtained by merging the SSMI and MODIS data: Geophysical Research Letters, v. 31, no. 18, L18103, doi:10.1029/2004GL020656.

Garcia, M.H., 2007, Sedimentation Engineering: Process, Measurement, Modeling, and Practice: Reston, Virginia, American Society of Civil Engineers, 1132 p.

Graf, W.L., 1988, Fluvial Processes in Dryland Rivers: Caldwell, New Jersey, Blackburn Press, 346 p.

Graves, S.D.B., McKay, C.P., Griffith, C.A., Ferri, F., and Fulchignoni, M., 2008, Rain and hail can reach the surface of Titan: Planetary and Space Science, v. 56, no. 3–4, p. 346–357, doi:10.1016/j.pss.2007.11.001.

Griffith, C.A., 2000, Detection of daily clouds on Titan: Science, v. 290, no. 5491, p. 509–513, doi:10.1126 /science.290.5491.509.

Hancock, G.S., Anderson, R.S., and Whipple, K.X., 1998, Beyond power: Bedrock river incision process and form, *in* Tinkler, J., and Wohl, E., eds., Rivers Over Rock: Fluvial Processes in Bedrock Channels: American Geophysical Union Geophysical Monograph 107, p. 35–60.

Haviv, I., Enzel, Y., Whipple, K.X., Zilberman, E., Stone, J., Matmon, A., and Fifield, L.K., 2006, Amplified erosion above waterfalls and oversteepened bedrock reaches: Journal of Geophysical Research, v. 111, F04004, doi:10.1029/2006JF000461.

Hayes, A.G., and 13 others, 2008, Hydrocarbon lakes on Titan: Distribution and interaction with a porous regolith: Geophysical Research Letters, v. 35, L09204, doi:09210.01029/02008GL033409.

Hayes, A.G., Wolf, A.S., Aharonson, O., Zebker, H., Lorenz, R., Kirk, R.L., Paillou, P., Lunine, J., Wye, L., Callahan, P., Wall, S., and Elachi, C., 2010, Bathymetry and absorptivity of Titan's Ontario Lacus: Journal of Geophysical Research, v. 115, no. E9, E09009, doi:10.1029 /2009JE003557.

Hayes, A.G., and 13 others, 2011, Transient surface liquid in Titan's polar regions from *Cassini*: Icarus, v. 211, no. 1, p. 655–671, doi:10.1016/j.icarus.2010.08.017.

Hess, M., 1966, Models and Analogies in Science: Notre Dame, Indiana, Notre Dame University Press, 184 p.

Horton, R., 1933, The role of infiltration in the hydrologic cycle: American Geophysical Union Transactions, v. 14, p. 446–460.

Horton, R., 1945, Erosional development of streams and their drainage basins; hydrophysical approach to quantitative morphology: Geological Society of America Bulletin, v. 56, no. 3, p. 275–370, doi:10.1130/0016-7606 (1945)56[275:EDOSAT]2.0.CO;2.

Howard, A., 1971, Optimal angles of stream junction: Geometric, stability to capture, and minimum power criteria: Water Resources Research, v. 7, no. 4, p. 863–873, doi:10.1029/WR007i004p00863.

Howard, A.D., 1967, Drainage analysis in geologic interpretation: A summation: American Association of Petroleum Geologists Bulletin, v. 51, p. 2246–2259.

Howard, A.D., 1988, Groundwater sapping experiments and modeling, *in* Craddock, R.A., ed., Sapping Features of the Colorado Plateau: A Comparative Planetary Geology Field Guide: Washington, D.C., National Aeronautics and Space Administration, p. 71–83.

Howard, A.D., and Kerby, G., 1983, Channel changes in badlands: Geological Society of America Bulletin, v. 94, no. 6, p. 739–752, doi:10.1130/0016-7606 (1983)94<739:CCIB>2.0.CO;2.

Howard, A.D., Dietrich, W.E., and Seidl, M.A., 1994, Modeling fluvial erosion on regional to continental scales: Journal of Geophysical Research–Solid Earth, v. 99, no. B7, p. 13,971–13,986, doi:10.1029/94JB00744.

Hueso, R., and Sánchez-Lavega, A., 2006, Methane storms on Saturn's moon Titan: Nature, v. 442, p. 428–431, doi:10.1038/nature04933.

Ichoku, C., and Chorowicz, J., 1994, A numerical approach to the analysis and classification of channel network patterns: Water Resources Research, v. 30, no. 2, p. 161–174, doi:10.1029/93WR02279.

Irwin, R.P., III, Craddock, R.A., and Howard, A.D., 2005, Interior channels in Martian valley networks: Discharge and runoff production: Geology, v. 33, p. 489–492, doi:10.1130/G21333.1.

Jacquemart, D., Lellouch, E., Bézard, B., De Bergh, C., Coustenis, A., Lacome, N., Schmitt, B., and Tomasko, M., 2008, New laboratory measurements of CH_4 in Titan's conditions and a reanalysis of the DISR near-surface spectra at the *Huygens* landing site: Planetary and Space Science, v. 56, no. 5, p. 613–623, doi:10.1016 /j.pss.2007.10.008.

Janssen, M.A., Lorenz, R.D., West, R., Paganelli, F., Lopes, R.M., Kirk, R.L., Elachi, C., Wall, S.D., Johnson, W.T.K., and Anderson, Y., 2009, Titan's surface at 2.2-cm wavelength imaged by the *Cassini* RADAR radiometer: Calibration and first results: Icarus, v. 200, no. 1, p. 222–239, doi:10.1016/j.icarus.2008.10.017.

Jaumann, R., and 18 others, 2008, Fluvial erosion and post-erosional processes on Titan: Icarus, v. 197, no. 2, p. 526–538, doi:10.1016/j.icarus.2008.06.002.

Jaumann, R., Kirk, R., Lorenz, R., Lopes, R., Stofan, E., Turtle, E., Keller, H., Wood, C., Sotin, C., and Soderblom, L., 2009, Geology and surface processes on Titan, *in* Brown, R., Waite, J., and Lebreton, J.-P., eds., Titan from *Cassini-Huygens*: New York, Springer, p. 75–140.

Karkoschka, E., and Tomasko, M.G., 2009, Rain and dewdrops on Titan based on in situ imaging: Icarus, v. 199, no. 2, p. 442–448, doi:10.1016/j.icarus.2008.09.020.

Karkoschka, E., Tomasko, M.G., Doose, L.R., See, C., McFarlane, E.A., Schröder, S.E., and Rizk, B., 2007, DISR imaging and the geometry of the descent of the *Huygens* probe within Titan's atmosphere: Planetary and Space Science, v. 55, no. 13, p. 1896–1935, doi:10.1016/j.pss.2007.04.019.

Kelessidis, V.C., 2004, An explicit equation for the terminal velocity of solid spheres falling in pseudoplastic liquids: Chemical Engineering Science, v. 59, p. 4437–4447, doi:10.1016/j.ces.2004.07.008.

Keller, H.U., Grieger, B., Küppers, M., Schröder, S.E., Skorov, Y.V., and Tomasko, M.G., 2008, The properties of Titan's surface at the *Huygens* landing site from DISR observations: Planetary and Space Science, v. 56, p. 728–752, doi:10.1016/j.pss.2007.11.020.

Kerridge, S.J., Flury, W., Horn, L.J., Lebreton, J.-P., Stetson, D.S., Stoller, R.L., and Tan, G.H., 1992, *Cassini*: Mission to Saturn and Titan: National Aeronautics and Space Administration Ames Research Center, Exobiology in Solar System Exploration, p. 229–248.

Khare, B.N., Sagan, C., Thompson, W.R., Arakawa, E.T., Meisse, C., and Tuminello, P.S., 1994, Optical properties of poly-HCN and their astronomical applications: Canadian Journal of Chemistry, v. 72, no. 3, p. 678–694, doi:10.1139/v94-093.

Knighton, D., 1998, Fluvial Forms and Processes: A New Perspective: New York, Oxford University Press, 383 p.

Kochel, R.C., 1988, Geomorphic impact of large floods: Review and new perspectives on magnitude and frequency, *in* Baker, V.R., Kochel, R.C., and Patton, P.C., eds., Flood Geomorphology: New York, Wiley Interscience, p. 169–187.

Komar, P.D., 1980, Modes of sediment transport in channelized water flows with ramifications to the erosion of the Martian outflow channels: Icarus, v. 42, p. 317–329, doi:10.1016/0019-1035(80)90097-4.

Lamb, M.P., and Dietrich, W.E., 2009, The persistence of waterfalls in fractured rock: Geological Society of America Bulletin, v. 121, p. 1123–1134, doi:10.1130/B26482.1.

Lamb, M.P., Dietrich, W.E., Perron, J.T., Howard, A.D., Johnson, J., and Whipple, K.X., 2006, Can springs cut canyons into rock?: Journal of Geophysical Research–Planets, v. 111, E07002, doi:10.1029/2005JE002663.

Lamb, M.P., Howard, A.D., Dietrich, W.E., and Perron, J.T., 2007, Formation of amphitheater-headed valleys by waterfall erosion after large-scale slumping on Hawai'i: Geological Society of America Bulletin, v. 119, no. 7–8, p. 805–822, doi:810.1130/B25986.

Lamb, M.P., Dietrich, W.E., Aciego, S.M., DePaolo, D.J., and Manga, M., 2008a, Formation of Box Canyon, Idaho, by megaflood: Implications for seepage erosion on Earth and Mars: Science, v. 320, no. 5879, p. 1067, doi:10.1126/science.1156630.

Lamb, M.P., Dietrich, W.E., and Sklar, L.S., 2008b, A model for fluvial bedrock incision by impacting suspended and bed load sediment: Journal of Geophysical Research, v. 113, no. F3, F03025, doi:10.1029/2007JF000915.

Lamb, M.P., Dietrich, W.E., and Venditti, J.G., 2008c, Is the critical Shields stress for incipient sediment motion dependent on channel-bed slope?: Journal of Geophysical Research, v. 113, no. F2, F02008, doi:10.1029/2007JF000831.

Langhans, M.H., and 13 others, 2012, Titan's fluvial valleys: Morphology, distribution, and spectral properties: Planetary and Space Science, v. 60, no. 1, p. 34–51, doi:10.1016/j.pss.2011.01.020.

Le Gall, A., Janssen, M.A., Paillou, P., Lorenz, R.D., and Wall, S.D., 2010, Radar-bright channels on Titan: Icarus, v. 207, no. 2, p. 948–958, doi:10.1016/j.icarus.2009.12.027.

Leopold, L.B., and Wolman, M.G., 1960, River meanders: Geological Society of America Bulletin, v. 71, p. 769–794, doi:10.1130/0016-7606(1960)71[769:RM]2.0.CO;2.

Litwin, K.L., Zygielbaum, B.R., Polito, P.J., Sklar, L.S., and Collins, G.C., 2012, Influence of temperature, composition and grain size on the tensile failure of water ice: Implications for erosion on Titan: Journal of Geophysical Research–Planets, v. 117, E08013, doi:10.1029/2012JE004101.

Lopes, R.M.C., and 43 others, 2007, Cryogenic features on Titan's surface as revealed by the *Cassini* Titan Radar Mapper: Icarus, v. 186, p. 395–412, doi:10.1016/j.icarus.2006.09.006.

Lopes, R.M.C., and 24 others, 2010, Distribution and interplay of geologic processes on Titan from *Cassini* Radar data: Icarus, v. 205, no. 2, p. 540–558, doi: 10.1016/j.icarus.2009.08.010.

Lorenz, R.D., 1993, The life, death and afterlife of a raindrop on Titan: Planetary and Space Science, v. 41, p. 647–655, doi:10.1016/0032-0633(93)90048-7.

Lorenz, R.D., 2000, The weather on Titan: Science, v. 290, no. 5491, p. 467–468, doi:10.1126/science.290.5491.467.

Lorenz, R.D., and Lunine, J.I., 1996, Erosion on Titan: Past and present: Icarus, v. 122, p. 79–91, doi:10.1006/icar.1996.0110.

Lorenz, R.D., and Lunine, J.I., 2006, Titan's damp ground: Constraints on Titan's surface thermal properties from the temperature evolution of the *Huygens* CGMS inlet: Meteoritical and Planetary Science, v. 41, p. 1–20.

Lorenz, R.D., and Rennó, N.O., 2002, Work output of planetary atmospheric engines: Dissipation in clouds and rain: Geophysical Research Letters, v. 29, no. 2, p. 1023, doi:10.1029/2001GL013771.

Lorenz, R.D., McKay, C.P., and Lunine, J.I., 1997, Photochemically driven collapse of Titan's atmosphere: Science, v. 275, p. 642–644, doi:10.1126/science.275.5300.642.

Lorenz, R.D., Griffith, C.A., Lunine, J.I., McKay, C.P., and Rennò, N.O., 2005, Convective plumes and the scarcity of Titan's clouds: Geophysical Research Letters, v. 32, L01201, doi:01210.01029/02004GL021415.

Lorenz, R.D., and 14 others, 2008a, Fluvial channels on Titan: Initial *Cassini* RADAR observations: Planetary and Space Science, v. 56, no. 8, p. 1132–1144, doi:10.1016/j.pss.2008.02.009.

Lorenz, R.D., West, R.D., and Johnson, W.T.K., 2008b, *Cassini* RADAR constraint on Titan's winter polar precipitation: Icarus, v. 195, no. 2, p. 812–816, doi:10.1016/j.icarus.2007.12.025.

Lorenz, R.D., Kargl, G., Ball, A.J., Zarnecki, J.C., Towner, M.C., Leese, M.R., McDonnell, J.A.M., Atkinson, K.R., Hathi, B., and Hagermann, A., 2009, Titan surface mechanical properties from the SSP ACC-I record of the impact deceleration of the *Huygens* probe, *in* Kargl, G., Kömle, N., Ball, A.J., and Lorenz, R.D., eds., Penetrometry in the Solar System II: Vienna, Austria, Austrian Academy of Sciences, p. 147–156.

Lorenz, R.D., Turtle, E.P., Stiles, B., Le Gall, A., Hayes, A., Aharonson, O., Wood, C.A., Stofan, E., and Kirk, R., 2011, Hypsometry of Titan: Icarus, v. 211, no. 1, p. 699–706, doi:10.1016/j.icarus.2010.10.002.

Lyell, C., 1830, Principles of Geology: An Attempt to Explain the Former Changes of the Earth's Surface, by Reference to Causes Now in Operation: London, Murray, 511 p.

Malin, M.C., and Edgett, K.S., 2003, Evidence for persistent flow and aqueous sedimentation on early Mars: Science, v. 302, no. 5652, p. 1931–1934, doi:10.1126/science.1090544.

Mars Channel Working Group, 1983, Channels and valleys on Mars: Geological Society of America Bulletin, v. 94, p. 1035–1054, doi:10.1130/0016-7606(1983)94<1035:CAVOM>2.0.CO;2.

Matson, D., Spilker, L., and Lebreton, J.-P., 2002, The *Cassini*/*Huygens* mission to the Saturnian system: Space Science Reviews, v. 104, p. 1–58, doi:10.1023/A:1023609211620.

McKay, C.P., Pollack, J.B., Lunine, J.I., and Courtin, R., 1993, Coupled atmosphere-ocean models of Titan's past: Icarus, v. 102, p. 88–98, doi:10.1006/icar.1993.1034.

Miller, M.C., McCave, I.N., and Komar, P.D., 1977, Threshold of sediment motion under unidirectional currents: Sedimentology, v. 41, p. 883–903.

Mitchell, J.L., 2008, The drying of Titan's dunes: Titan's methane hydrology and its impact on atmospheric circulation: Journal of Geophysical Research, v. 113, no. E8, doi:10.1029/2007JE003017.

Mitchell, J.L., Pierrehumbert, R.T., Frierson, D.M.W., and Caballero, R., 2006, The dynamics behind Titan's methane clouds: Proceedings of the National Academy of Sciences of the United States of America, v. 103, no. 49, p. 18,421–18,426, doi:10.1073/pnas.0605074103.

Mitchell, J.L., Ádámkovics, M., Caballero, R., and Turtle, E.P., 2011, Locally enhanced precipitation organized by planetary-scale waves on Titan: Nature Geoscience, v. 4, no. 9, p. 589–592, doi:10.1038/ngeo1219.

Mitri, G., Showman, A.P., Lunine, J.I., and Lorenz, R.D., 2007, Hydrocarbon lakes on Titan: Icarus, v. 186, p. 385–394, doi:10.1016/j.icarus.2006.09.004.

Montgomery, D.R., and Buffington, J.M., 1997, Channel-reach morphology in mountain drainage basins: Geological Society of America Bulletin, v. 109, no. 5, p. 596–611, doi:10.1130/0016-7606(1997)109<0596:CRMIMD>2.3.CO;2.

Moore, J.M., and Howard, A.D., 2010, Are the basins of Titan's Hotei Regio and Tui Regio sites of former low latitude seas?: Geophysical Research Letters, v. 37, no. 22, L22205, doi:10.1029/2010GL045234.

Moore, J.M., and Pappalardo, R.T., 2011, Titan: An exogenic world?: Icarus, v. 212, no. 2, p. 790–806, doi:10.1016/j.icarus.2011.01.019.

Moore, J.M., Howard, A.D., Dietrich, W.E., and Schenk, P.M., 2003, Martian layered fluvial deposits: Implications for Noachian climate scenarios: Geophysical Research Letters, v. 30, no. 24, p. 2292, doi:10.1029/2003GL019002.

Mutch, T.A., 1979, Planetary surfaces: Reviews of Geophysics and Space Physics, v. 17, p. 1694–1722, doi:10.1029/RG017i007p01694.

Nanson, G.C., Tooth, S., and Knighton, A.D., 2002, A global perspective on dryland rivers: Perceptions, misconceptions and distinctions, *in* Bull, L.J., and Kirkby, M.J., eds., Dryland Rivers: Hydrology and Geomorphology of Semi-Arid Channels: Chichester, UK, Wiley, p. 17–54.

Nelson, R.M., and 32 others, 2009a, Photometric changes on Saturn's Titan: Evidence for active cryovolcanism: Geophysical Research Letters, v. 36, no. 4, L04202, doi:10.1029/2008GL036206.

Nelson, R.M., and 28 others, 2009b, Saturn's Titan: Surface change, ammonia, and implications for atmospheric and tectonic activity: Icarus, v. 199, no. 2, p. 429–441, doi:10.1016/j.icarus.2008.08.013.

Niemann, H.B., and 17 others, 2005, The abundances of constituents of Titan's atmosphere from the GCMS instrument on the *Huygens* probe: Nature, v. 438, no. 7069, p. 779–784, doi:10.1038/nature04122.

Nikuradse, J., 1933, Stromungsgesetze in rauhen Rohren: Forschung auf dem Gebiete des Ingenieurwesens, v. 361, p. 22.

Parker, G., 1990, Surface-based bedload transport relation for gravel rivers: Journal of Hydraulic Research, v. 28, no. 4, p. 417–436, doi:10.1080/00221689009499058.

Parker, G., 1991, Selective sorting and abrasion of river gravel: II. Applications: Journal of Hydraulic Engineering, v. 117, no. 2, p. 150–171, doi:10.1061/(ASCE)0733-9429(1991)117:2(150).

Parker, G., Klingeman, P.C., and McLean, D.G., 1982, Bedload and size distribution in paved gravel-bed streams: Journal of the Hydraulics Division, v. 108, no. 4, p. 544–571.

Parker, G., Wilcock, P.R., Paola, C., Dietrich, W.E., and Pitlick, J., 2007, Physical basis for quasi-universal relations describing bankfull hydraulic geometry of single-thread gravel bed rivers: Journal of Geophysical Research–Earth Surface, v. 112, doi:10.1029/2006JF000549.

Perron, J.T., and de Pater, I., 2004, Dynamics of an ice continent on Titan: Geophysical Research Letters, v. 31, L17S04, doi:10.1029/2004GL019802.

Perron, J.T., and Hamon, J.L., 2012, Equilibrium form of horizontally retreating, soil-mantled hillslopes: Model

development and application to a groundwater sapping landscape: Journal of Geophysical Research, v. 117, no. F1, F01027, doi:10.1029/2011JF002139.

Perron, J.T., Lamb, M.P., Koven, C.D., Fung, I.Y., Yager, E., and Adamkovics, M., 2006, Valley formation and methane precipitation rates on Titan: Journal of Geophysical Research–Planets, v. 111, no. E11, doi:10.1029/2005je002602.

Pieri, D.C., 1979, Morphology of Martian Valleys [Ph.D. dissertation]: Ithaca, New York, Cornell University, 305 p.

Polito, P.J., Litwin, K.L., Zygielbaum, B.R., Sklar, L.S., and Collins, G.C., 2009, Experimental investigation of the temperature dependence of polycrystalline ice strength and resistance to low-velocity impacts with application to Titan: Eos (Transactions, American Geophysical Union), v. 90, no. 52, Fall Meeting supplement, Abstract P23E-06.

Porco, C.C., and 19 others, 2004, *Cassini* imaging science: Instrument characteristics and anticipated scientific investigations at Saturn: Space Science Reviews, v. 115, p. 363–497, doi:10.1007/s11214-004-1456-7.

Porco, C.C., and 35 others, 2005, Imaging of Titan from the *Cassini* spacecraft: Nature, v. 434, no. 7030, p. 159–168, doi:10.1038/nature03436.

Radebaugh, J., Lorenz, R.D., Kirk, R.L., Lunine, J.I., Stofan, E.R., Lopes, R.M.C., and Wall, S.D., and the *Cassini* Radar Team, 2007a, Mountains on Titan observed by *Cassini* Radar: Icarus, v. 192, p. 77–91, doi:10.1016/j.icarus.2007.06.020.

Radebaugh, J., and 14 others, 2007b, Dunes on Titan observed by *Cassini* Radar: Icarus, v. 194, p. 690–703, doi:10.1016/j.icarus.2007.1010.1015.

Radebaugh, J., and 20 others, 2011, Regional geomorphology and history of Titan's Xanadu province: Icarus, v. 211, no. 1, p. 672–685, doi:10.1016/j.icarus.2010.07.022.

Rannou, P., Montmessin, F., Hourdin, F., and Lebonnois, S., 2006, The latitudinal distribution of clouds on Titan: Science, v. 311, no. 5758, p. 201–205, doi:10.1126/science.1118424.

Rodriguez, S., and 13 others, 2009, Global circulation as the main source of cloud activity on Titan: Nature, v. 459, no. 7247, p. 678–682, doi:10.1038/nature08014.

Rodriguez, S., Le Mouélic, S., Rannou, P., Sotin, C., Brown, R.H., Barnes, J.W., Griffith, C.A., Burgalat, J., Baines, K.H., Buratti, B.J., Clark, R.N., and Nicholson, P.D., 2011, Titan's cloud seasonal activity from winter to spring with *Cassini*/VIMS: Icarus, v. 216, no. 1, p. 89–110, doi:10.1016/j.icarus.2011.07.031.

Roe, H.G., de Pater, I., Macintosh, B.A., and McKay, C.P., 2002, Titan's clouds from *Gemini* and Keck Adaptive Optics Imaging: The Astrophysical Journal, v. 581, p. 1399–1406, doi:10.1086/344403.

Rubin, D.M., and Hesp, P.A., 2009, Multiple origins of linear dunes on Earth and Titan: Nature Geoscience, v. 2, p. 653–658, doi:10.1038/ngeo610.

Schaller, E.L., Brown, M.E., Roe, H.G., and Bouchez, A.H., 2006, A large cloud outburst at Titan's south pole: Icarus, v. 182, no. 1, p. 224–229, doi:10.1016/j.icarus.2005.12.021.

Schlichting, H., 1979, Boundary-Layer Theory: New York, McGraw-Hill, 747 p.

Schneider, T., Graves, S.D.B., Schaller, E.L., and Brown, M.E., 2012, Polar methane accumulation and rainstorms on Titan from simulations of the methane cycle: Nature, v. 481, no. 7379, p. 58–61, doi:10.1038/nature10666.

Schröder, S., and Keller, H., 2008, The reflectance spectrum of Titan's surface at the *Huygens* landing site determined by the descent imager/spectral radiometer: Planetary and Space Science, v. 56, no. 5, p. 753–769, doi:10.1016/j.pss.2007.10.011.

Schulson, E.M., and Duval, P., 2009, Creep and Fracture of Ice: London, Cambridge University Press, 391 p.

Schumm, S., 1956, Evolution of drainage systems and slopes in badlands at Perth Amboy, New Jersey: Geological Society of America Bulletin, v. 67, no. 5, p. 597–646, doi:10.1130/0016-7606(1956)67[597:EODSAS]2.0.CO;2.

Schumm, S.A., 1991, To Interpret the Earth: Ten Ways to be Wrong: Cambridge, UK, Cambridge University Press, 133 p.

Schumm, S.A., Boyd, K.F., Wolff, C.G., and Spitz, W.J., 1995, A ground-water sapping landscape in the Florida Panhandle: Geomorphology, v. 12, no. 4, p. 281–297, doi:10.1016/0169-555X(95)00011-S.

Shields, A., 1936, Application of Similarity Principles and Turbulence Research to Bed-Load Movement: Pasadena, California, U.S. Department of Agriculture Soil Conservation Service Cooperative Laboratory, California Institute of Technology, Hydrodynamics Laboratory Publication, 47 p.

Sklar, L.S., and Dietrich, W.E., 2001, Sediment and rock strength controls on river incision into bedrock: Geology, v. 29, no. 12, p. 1087–1090, doi:10.1130/0091-7613(2001)029<1087:SARSCO>2.0.CO;2.

Sklar, L.S., and Dietrich, W.E., 2004, A mechanistic model for river incision into bedrock by saltating bed load: Water Resources Research, v. 40, no. W06301, doi:10.1029/2003WR002496.

Sklar, L.S., and Dietrich, W.E., 2006, The role of sediment in controlling steady-state bedrock channel slope: Implications of the saltation–abrasion incision model: Geomorphology, v. 82, p. 58–83, doi:10.1016/j.geomorph.2005.08.019.

Soderblom, L.A., and 26 others, 2007a, Correlations between *Cassini* VIMS spectra and RADAR SAR images: Implications for Titan's surface composition and the character of the *Huygens* probe landing site: Planetary and Space Science, v. 55, p. 2025–2036, doi:10.1016/j.pss.2007.04.014.

Soderblom, L.A., and 18 others, 2007b, Topography and geomorphology of the *Huygens* landing site on Titan: Planetary and Space Science, v. 55, p. 2015–2024, doi:10.1016/j.pss.2007.04.015.

Soderblom, L.A., Barnes, J.W., Brown, R.H., Clark, R.N., Janssen, M.A., McCord, T.B., Niemann, H.B., and Tomasko, M.G., 2009, Composition of Titan's surface, *in* Brown, R.H., Lebreton, J.-P., and Waite, J.H., Jr., eds., Titan from *Cassini-Huygens*: Dordrecht, Heidelberg, Springer, p. 141–175.

Sotin, C., and 25 others, 2005, Release of volatiles from a possible cryovolcano from near-infrared imaging of Titan: Nature, v. 435, no. 7043, p. 786–789, doi:10.1038/nature03596.

Southard, J.B., 1991, Experimental determination of bedform stability: Annual Review of Earth and Planetary Sciences, v. 19, p. 423–455, doi:10.1146/annurev.ea.19.050191.002231.

Southard, J.B., and Boguchwal, L.A., 1990a, Bed configurations in steady unidirectional water flows: 2. Synthesis of flume data: Journal of Sedimentary Petrology, v. 60, no. 5, p. 658–679.

Southard, J.B., and Boguchwal, L.A., 1990b, Bed configurations in steady unidirectional water flows: 3. Effects of temperature and gravity: Journal of Sedimentary Petrology, v. 60, no. 5, p. 680–686.

Stock, J.D., and Dietrich, W.E., 2006, Erosion of steepland valleys by debris flows: Geological Society of America Bulletin, v. 118 no. 9/10, p. 1125–1148, doi: 10.1130/B25902.1.

Stofan, E.R., and 37 others, 2007, The lakes of Titan: Nature, v. 445, no. 7123, p. 61–64, doi:10.1038/nature05438.

Tokano, T., 2009, Impact of seas/lakes on polar meteorology of Titan: Simulation by a coupled GCM-Sea model: Icarus, v. 204, no. 2, p. 619–636, doi:10.1016/j.icarus.2009.07.032.

Tokano, T., 2011, Precipitation climatology on Titan: Science, v. 331, no. 6023, p. 1393–1394, doi:10.1126/science.1204092.

Tokano, T., Neubauer, F.M., Laube, M., and McKay, C.P., 2001, Three-dimensional modeling of the tropospheric methane cycle on Titan: Icarus, v. 153, p. 130–147, doi:10.1006/icar.2001.6659.

Tokano, T., McKay, C.P., Neubauer, F.M., Atreya, S.K., Ferri, F., Fulchignoni, M., and Niemann, H.B., 2006, Methane drizzle on Titan: Nature, v. 442, p. 432–435, doi:10.1038/nature04948.

Tomasko, M.G., and 38 others, 2005, Rain, wind, and haze during the *Huygens* probe's descent to Titan's surface: Nature, v. 438, p. 765–778, doi:10.1038/nature04126.

Toon, O.B., McKay, C.P., Courtin, R., and Ackerman, T.P., 1988, Methane rain on Titan: Icarus, v. 75, p. 255–284, doi:10.1016/0019-1035(88)90005-X.

Turtle, E.P., Perry, J.E., McEwen, A.S., DelGenio, A.D., Barbara, J., West, R.A., Dawson, D.D., and Porco, C.C., 2009, *Cassini* imaging of Titan's high-latitude lakes, clouds, and south-polar surface changes: Geophysical Research Letters, v. 36, no. 2, doi:10.1029/2008GL036186.

Turtle, E.P., and 13 others, 2011, Rapid and extensive surface changes near Titan's equator: Evidence of April showers: Science, v. 331, p. 1414–1417, doi:10.1126/science.1201063.

Turton, R., and Clark, N.N., 1987, An explicit relationship to predict spherical particular terminal velocity: Powder Technology, v. 53, p. 127–129, doi:10.1016/0032-5910(87)85007-6.

Twidale, C.R., 2004, River patterns and their meaning: Earth-Science Reviews, v. 67, no. 3-4, p. 159–218, doi:10.1016/j.earscirev.2004.03.001.

van den Berg, J.H., and van Gelder, A., 1993, A new bedform stability diagram, with emphasis on the transition of ripples to plane bed in flows over fine sand and silt, *in* Marzo, M., and Puigdefábregas, C., eds., Alluvial Sedimentation: International Association of Sedimentologists Special Publication 17: Oxford, UK, Blackwell Scientific Publications, p. 11–21.

Vanoni, V.A., 1974, Factors determining bed form of alluvial streams: Journal of Hydraulic Engineering, American Society of Civil Engineers (ASCE), v. 100, p. 363–378.

van Rijn, L.C., 1984, Sediment transport: Part III. Bed forms and alluvial roughness: Journal of Hydraulic Engineering, American Society of Civil Engineers (ASCE), v. 110, p. 1613–1641.

Waite, J.H., Jr., Young, D.T., Westlake, J.H., Lunine, J.I., McKay, C.P., and Lewis, W.S., 2009, High-altitude production of Titan's aerosols, *in* Brown, R.H., Lebreton, J.-P., and Waite, J.H., Jr., eds., Titan from *Cassini-Huygens*: Dordrecht, Heidelberg, Springer, p. 201–214.

Wall, S., Hayes, A., Bristow, C., Lorenz, R., Stofan, E., Lunine, J, Le Gall, A., Janssen, M., Lopes, R., Wye, L., Soderblom, L., Paillou, P., Aharonson, O., Zebker, H., and Farr, T., Mitri, G, Kirk, R., Mitchell, K., Notarnicola, C., Casarano, D., and Ventura, B., 2010, Active shoreline of Ontario Lacus, Titan: A morphological study of the lake and its surroundings: Geophysical Research Letters, v. 37, L05202, doi:10.1029/2009GL041821.

Wall, S.D., and 16 others, 2009, *Cassini* RADAR images at Hotei Arcus and western Xanadu, Titan: Evidence for geologically recent cryovolcanic activity: Geophysical Research Letters, v. 36, no. 4, doi:10.1029/2008GL036415.

Wang, C.C., Lang, E.K., and Signorell, R., 2010, Methane gas stabilizes supercooled ethane droplets in Titan's clouds: The Astrophysical Journal Letters, v. 712, no. 1, p. L40–L43, doi:10.1088/2041-8205/712/1/L40.

Ward, R.C., 1984, On the response to precipitation of headwater streams in humid areas: Journal of Hydrology (Amsterdam), v. 74, p. 171–189, doi:10.1016/0022-1694(84)90147-1.

Whipple, K.X., 2004, Bedrock rivers and the geomorphology of active orogens: Annual Review of Earth and Planetary Sciences, v. 32, p. 151–185, doi:10.1146/annurev.earth.32.101802.120356.

Whipple, K.X., and Tucker, G.E., 1999, Dynamics of the stream-power river incision model: Implications for height limits of mountain ranges, landscape response timescales, and research needs: Journal of Geophysical Research, v. 104, no. B8, p. 17,661–17,674, doi:10.1029/1999JB900120.

Whipple, K.X., Hancock, G.S., and Anderson, R.S., 2000, River incision into bedrock: Mechanics and relative efficacy of plucking, abrasion, and cavitation: Geological Society of America Bulletin, v. 112, no. 3, p. 490–503, doi:10.1130/0016-7606(2000)112<490:RIIBMA>2.0.CO;2.

White, S.J., 1970, Plane bed thresholds of fine grained sediments: Nature, v. 228, no. 5267, p. 152–153, doi:10.1038/228152a0.

Wiberg, P.L., and Smith, J.D., 1987, Calculations of the critical shear-stress for motion of uniform and heterogeneous sediments: Water Resources Research, v. 23, no. 8, p. 1471–1480, doi:10.1029/WR023i008p01471.

Wilcock, P.R., 1993, Critical shear-stress of natural sediments: Journal of Hydraulic Engineering, v. 119, no. 4, p. 491–505, doi:10.1061/(ASCE)0733-9429(1993)119:4(491).

Wilcock, P.R., and Crowe, J.C., 2003, Surface-based transport model for mixed-size sediment: Journal of Hydraulic Engineering, v. 129, p. 120–128, doi:10.1061/(ASCE)0733-9429(2003)129:2(120).

Williams, G.P., 1988, Paleofluvial estimates from dimensions of former channels and meanders, *in* Baker, V.R., ed., Flood Geomorphology: New York, Wiley, p. 321–334.

Wohl, E.E., 2000, Mountain Rivers: Washington, D.C., American Geophysical Union Press, 315 p.

Wood, C.A., Lunine, J.I., Stofan, E., Lorenz, R., Lopes, R., Radebaugh, J., Wall, S.D., Paillou, P., Farr, T., and the RADAR Science Team., 2008, Degraded impact craters on Titan: Proceedings of the Lunar and Planetary Science Conference XXXIX: Houston, Texas, Lunar and Planetary Institute, Abstract 1990.

Yair, A., and Lavee, H., 1985, Runoff generation in arid and semi-arid zones, *in* Anderson, M.G., and Burt, T.P., eds., Hydrological Forecasting: Chichester, UK, John Wiley and Sons, p. 183–220.

Yung, Y.L., Allen, M., and Pinto, J.P., 1984, Photochemistry of the atmosphere of Titan—Comparison between model and observations: The Astrophysical Journal, Supplement Series, v. 55, p. 465–506, doi:10.1086/190963.

Zarnecki, J.C., and 25 others, 2005, A soft solid surface on Titan as revealed by the *Huygens* Surface Science Package: Nature, v. 438, no. 7069, p. 792–795, doi:10.1038/nature04211.

Science Editor: Christian Koeberl

Manuscript Received 23 September 2011
Revised Manuscript Received 18 July 2012
Manuscript Accepted 28 July 2012

Printed in the USA